ELECTRODEPOSITION OF NiW ALLOYS INTO DEEP RECESSES

A Thesis

Submitted to the Graduate Faculty of the
Louisiana State University and
Agricultural and Mechanical College
in partial fulfillment of the requirements for the degree of
Master of Science in Chemical Engineering

in

The Department of Chemical Engineering

by
Lakshmikanth Namburi
B.Tech., Osmania University, 1999
December 2001

To my loving parents,

Krishna Kumar Namburi and Savitri Namburi

ACKNOWLEDGEMENTS

I sincerely thank my graduate advisor Dr. E. J. Podlaha for patiently guiding me through this exciting project.

I thank Dr. R. L. McCarley, and Dr. K. W. Kelly for accepting my invitation to be on my graduate committee.

I thank the Defense Advanced Research projects Agency (DARPA) for funding this study.

My sincere thanks also go to Dr. X. Xie with the LSU Geology Department for microprobe analyses and SEM micrographs, Mr. Rick Young for micropolishing, Mr. Varshini Singh for microhardness test, Mr. Paul Rodriguez and Mr. Frederick McKenzie for substrate jig preparation, Dr. Tao Wang for sample mounting.

I would also like to acknowledge the support I received from my colleagues in the electrochemical-engineering laboratory Amrit Panda, Anirban Mukherjee, Raymond Husser, Qiang Huang, Yun Zhuang, Patrick, Gaby.

TABLE OF CONTENTS

ACKNOWLEDGEMENTS iii

LIST OF FIGURES v

ABSTRACT viii

CHAPTER 1. INTRODUCTION 1

CHAPTER 2. LITERATURE REVIEW 3
- 2.1 Nickel-Tungsten Properties and Uses 3
- 2.2 Plating Parameters 3
- 2.3 Deep Recess Plating 6

CHAPTER 3. STATEMENT OF PURPOSE 9

CHAPTER 4. EXPERIMENTAL 10
- 4.1 Electrolytes Used 10
- 4.2 Substrate Preparation 11
- 4.3 Cell Design and Operation 11
- 4.4 Experimental Procedure 14
- 4.5 Deposit Analysis 17

CHAPTER 5. RESULTS AND DISCUSSION 19
- 5.1 Choice of Electrolyte 19
  - 5.1.1 Sulfamate Bath 19
  - 5.1.2 Citrate Bath 19
- 5.2 Deep Recess Plating 22
  - 5.2.1 Potentiostatic Pulsing 23
  - 5.2.2 Constant Current Pulsing 25
  - 5.2.3 Galvanostatic Step Ramp Pulsing 27
  - 5.2.4 Constant Current Pulsing with Reduction in 'Off' Time with Time 30
- 5.3 Ramping Scheme to Electrodeposit Ni into Deep Recesses 31
- 5.4 Pulsing Scheme to Electrodeposit Ni-Fe Alloy into Deep Recesses 33
- 5.5 Experiments on Rotating Cylinder Electrodes 34
- 5.6 Effect of Ni Concentration on NiW Electrodeposition 36
- 5.7 Effect of Tungstate Concentration on NiW Electrodeposition 36

CHAPTER 6. CONCLUSION 39

REFERENCES 40

VITA 42

LIST OF FIGURES

Figure 4.1 Schematic of recessed substrate preparation with x-ray exposure at CAMD 12

Figure 4.2 Schematic of the cell used for deep recess plating 14

Figure 4.3 Schematic of the cell with RCE, platinum anode, and SCE reference electrode. 15

Figure 4.4 A schematic of the pulsing scheme for deep recess electrodeposition.......... 15

Figure 5.1: Weight percent tungsten against applied current density at 300 rpm for sulfamate bath, pH of 7, at 60 °C 19

Figure 5.2: Current efficiency vs. applied current density at 300 rpm for sulfamate bath, pH of 7, at 60 °C 20

Figure 5.3: Partial current densities of Ni, W and side reaction as a function of potential at 300 rpm for sulfamate bath, pH of 7, at 60 °C 20

Figure 5.4: Weight Percent W as a function of applied current density for Bath #1 (Equimolar) at 300 rpm, pH of 10, at 70 °C.. 21

Figure 5.5: Current efficiency as a function of applied current density for Bath #1 (Equimolar) at 300 rpm, pH of 10, at 70 °C.. 21

Figure 5.6: Partial current densities of Ni, W, side reactions as a function of potential for Bath #1 (Equimolar) at 300 rpm, pH of 10, at 70 °C. 22

Figure 5.7 Schematic of the pulsing scheme used for deep recess plating 23

Figure 5.8: SEM micrograph of Ni-W microposts obtained by potentiostatic pulsing from Bath #3, pH of 10, at 70 °C. ‘On’ potential: -1.15 V vs. SCE ‘Off’ potential: open circuit.. 24

Figure 5.9: SEM Micrograph of Ni-W microposts obtained by potentiostatic pulsing from Bath #3, pH of 10, at 70 °C. ‘On’ potential: -1.25 V vs. SCE 24

Figure 5.10: SEM micrograph of Ni-W microposts obtained by potentiostatic pulsing from Bath #3, pH of 10, at 70 °C. ‘On’ potential: -1.3 V vs. SCE 24

Figure 5.11: Optical picture of the Ni-W microposts deposited from Bath #4 by potentiostatic pulsing with pulse potential of –1.2 V, ‘on’ time of 30 sec and off time of ’60’ sec.. 25

Figure 5.12: Optical picture of 200 μm tall microposts obtained from Bath #4 by constant current pulsing with a duty cycle of 0.2, pulse current of 16.5 mA/cm^2. 26

Figure 5.13: SEM image of a micropost obtained from Bath #4 by constant current pulsing with a duty cycle of 0.2, pulse current of 16.5 mA/cm^2. 26

Figure 5.14: SEM micrograph of microposts grown half way, obtained from Bath #4 by constant current pulsing with a duty cycle of 0.25, pulse current of 17.5 mA/cm^2. .. 27

Figure 5.15 Uniform composition gradient along the length of the microposts obtained from Bath #4 by constant current pulsing with a duty cycle of 0.25, pulse current of 17.5 mA/cm^2.. 27

Figure 5.16: Schematic of galvanostatic step ramp pulsing. 28

Figure 5.17: SEM image of 500 µm tall microposts' cross-section obtained from Bath #4 by galvanostatic step ramp pulsing with a duty cycle of 0.25.................................... 29

Figure 5.18: Weight percent W along the length of the microposts obtained from Bath #4 by galvanostatic step ramp pulsing with a duty cycle of 0.25.................................... 29

Figure 5.19: SEM micrograph of of 500 µm tall microposts' cross-section obtained from Bath #4 by galvanostatic step ramp pulsing with a duty cycle of 0.25. 30

Figure 5.20: Weight percent W along the length of the microposts obtained from Bath #4 by galvanostatic step ramp pulsing with a duty cycle of 0.25.................................... 30

Figure 5.21: Schematic of the Pulsing Scheme showing 'Off' Time Reduction with Time 31

Figure 5.22: Microprobe analysis showing composition gradients in the microposts obtained by 'off' time reduction scheme.. 31

Figure 5.23: Schematic of the ramping scheme used to plate Ni into 500 µm recesses.. 32

Figure 5.24: SEM micrograph of Ni microposts obtained from sulfamate bath by using the ramping scheme in Figure 5.22 32

Figure 5.25: SEM image of 100 µm tall Ni-Fe Microposts with 58 % Fe obtained by Pulse Plating.. 33

Figure 5.26: SEM image of 500 µm tall Ni-Fe Microposts with 64 % Fe obtained by Pulse Plating.. 34

Figure 5.27: Weight percent tungsten vs. applied current density at rotation rates of 100, 700, 1300 and 1900 rpm for Bath #4, (Intermediate), pH of 10, at 70 °C. 34

Figure 5.28: Current efficiency vs. applied current density at rotation rates of 100, 700, 1300 and 1900 rpm for Bath #4, (Intermediate), pH of 10, at 70 °C. 35

Figure 5.29: Partial current densities of Ni and W vs. potential at rotation rates of 100,700, 1300 and 1900 rpm for Bath #3, (Intermediate), pH of 10, at 70 °C. 35

Figure 5.30: Partial Current Densities of Side Reaction vs. Potential at rotation rates of 100, 700, 1300 and 1900 rpm for Bath #3, (Intermediate), pH of 10, at 70 °C. 36

Figure 5.31: Weight Percent W vs. Current Density for Bath #1, Bath #3 and Bath #4 at 300 rpm, pH of 10, and at 70 °C 37

Figure 5.32: Current Efficiency vs. Current Density for Bath #1, Bath #3 and Bath #4 at 300 rpm, pH of 10, and at 70 °C, different Ni concentrations of the electrolyte 37

Figure 5.33: Weight Percent W as a function of applied current density for Bath #2 (Double Tungsten) at 300 rpm, pH of 10, at 70 °C. 38

Figure 5.34: Current efficiency as a function of applied current density for Bath #2 (Double Tungsten) at 300 rpm, pH of 10, at 70 °C. 38

ABSTRACT

Pulse electrodeposition has been investigated as a general technique for the electrodeposition of nickel-tungsten alloys in deep recesses for MEMS. Ni-W exhibits an induced codeposition mechanism, where the Ni reaction rate enhances the codeposition of W. Electrodeposition of this alloy has been achieved into recesses of 500 micron deep. The challenges that have been encountered are those related to gas evolving side reactions, local pH rises, diffusional limitations of the soluble species and long times required for filling the recesses.

Electrodeposition on cylinder electrodes at different rotation rates was also carried out in order to obtain data on composition of the alloy and current efficiency of the process, for different baths considered. These studies were carried out to examine the suitability of the bath for microstructure development and to describe better how the codeposition processes is affected by mass transport.

CHAPTER 1. INTRODUCTION

Micro Electronic Mechanical Systems (MEMS) is a burgeoning new technology, which exploits the existing microelectronics infrastructure to create complex machines with micron feature sizes. These machines can have many functions, including sensing, communication and actuation.

The miniature components for these machines often require electrodeposition fabrication steps into deep recesses produced by x-ray lithography or photolithography. Electrodeposited nickel is one of the most widely employed materials in the fabrication of micromachines, such as micro-gears, micro-cantilevers, etc., and their components. However, the use of Ni is limited when properties like mechanical strength, thermal stability, hardness, wear and corrosion resistance, are desired. Alloys provide the obvious alternatives, as their properties can be tailored with different combinations of metals and compounds.

Significant research has gone into plating different alloys from a wide variety of electrolytes onto flat, unrecessed surfaces. But, those findings do not always translate into recesses of different geometries and sizes. This is exactly the case with Ni-W alloys. The major limiting factor for the adaptability of conventional plating baths to deep recess plating is the variance in hydrodynamic conditions. Despite electrolyte agitation at the mouth of the recess, the electrolyte in the recess remains stagnant creating transport limitations of the reactant species. In addition, reactions inherent with the mechanism of alloy electrodeposition also produce side products. For example, H_2 and hydroxyl ions from water reduction are commonly generated products from side reactions. The hydroxyl ions generated could raise the pH in the recess and alter the solution equilibria affecting the electrodeposition reactions.

A study on the electrodeposition of Ni-W alloy into deep recesses of 500 microns is presented here. Nickel-tungsten alloys have the capability to significantly enhance the hardness and wear resistance of microstructures, coupled with high thermal resistance.[1] Tungsten with its unusual properties such as, highest melting point (3410 °C) of all metals, lowest coefficient of linear thermal expansion (4.3×10^{-6}/°C), highest tensile strength (410 kg/mm^2 or 590000 lb/in^2) and one of the highest Young's modulus of elasticity (3500 kg/mm^2 or 5×10^7 lb/in^2), can render excellent properties to its alloy. Tungsten alloys have many potential applications. They could replace hard chromium coatings, as chromates are known to be highly toxic and carcinogenic. Krishnan *et al.*[2] investigated Ni-W alloy as a possible alternative for hard chromium. The use of hexavalent chromates requires special waste disposal, expensive breathing apparatuses and exhaust systems. As tungsten alloy baths are found to possess more throwing power, W can be more easily deposited for miniature features than chromium, and would be a major improvement to existing Ni microstructures.

The LIGA technique (German acronym: Lithograhie, Galvanoforming, Abformung) is being widely used to generate microstructures with high aspect ratios.[3] The process consists of a lithographic step during which an absorber pattern is transferred to a resist layer by shadow printing with synchrotron radiation. This is followed by electroplating into the recessed pattern. The electroplated microstructures can then be used as final products or as mold inserts to replicate structures through processes like injection molding, reaction injection molding, hot-embossing, slip casting or

extrusion.[1,3,4,5] Lowe *et al.*[1] reported the fabrication of a 50 micron thick Ni-W alloy micro-gear wheel with high microhardness using a weak alkaline sulfate electrolyte and a wetting agent. Although, no study has demonstrated much thicker micro-deposits on the order of 100s of microns. Electrodeposition of tungsten alloys into deep recesses is expected to be a challenge due to the large hydroxyl ion generation that increases the electrode surface pH during continuous deposition conditions.

It is a well-established fact that tungsten cannot be electrodeposited from aqueous electrolytes, but can be codeposited with iron group elements such as nickel to form an alloy.[6,7] This is classified as induced codeposition. Existing literature on the reaction mechanism varies between authors and is contradictory. Brenner[6] presented several hypotheses such as, a catalytic influence of the cathodic surface codeposition, formation of an internal orbital complex in the electrolyte, ennobling of the deposition potential as a result of the alloy deposited, formation of an active complex on the cathode, and an increase of the "equilibrium" solubility of tungsten. Tungsten alloys usually electrodeposit at potentials more positive than those at which the iron group elements deposit. Of the many plating baths proposed for electroplating Ni-W, sulfamate[8] and ammoniacal citrate[9] baths are the most widely used.

There are several problems anticipated with the electrodeposition of Ni-W alloys into deep recesses such as the influence of the side reaction previously mentioned. Additionally, the deposition of tungsten also generates hydroxyl ions that in combination with the side reaction contribute to a local pH rise. The pH rise is expected to alter the concentration in the deposit, and morphology. One method to minimize the local pH rise is through the use of pulsing techniques such as galvanostatic pulsing, and galvanostatic step ramping while pulsing, as presented in this thesis.

CHAPTER 2. LITERATURE REVIEW

2.1 Nickel-Tungsten Properties and Uses

Tungsten alloys are known for their excellent mechanical and tribological properties. Lowe, *et al.*[1] found that the hardness of Ni-W alloys is two to three times higher than that of pure electrodeposited Ni. Nickel-tungsten layers with 10-weight % W resulted in microhardness (Vickers hardness) of 600 HV. Annealing to 650 ºC produced values up to 800 HV. Using metallic microstructures as mold inserts for hot embossing and injection molding requires hard and wear resistant materials in order to achieve an exact replication into polymers and ceramics. The hardness and thermal stability of mold inserts were found to increase significantly with nickel-tungsten alloys. Lowe, *et al.* also reported that nickel-tungsten alloys were employed for the manufacture of microstructured tools due to their excellent mechanical properties regarding wear and mechanical durability. These tools have found applications in hot embossing and injection molding processes. As previously noted, Younes *et al.*[10] indicated that the concentration of W in the plated alloy, has a major effect on the mechanical and chemical properties, such as hardness, abrasion resistance, and improved corrosion resistance at high temperatures. Also, Singh, *et al.*[11] reported that the microhardness of Ni-W deposits was found to increase with an increase in tungsten content in the alloy.

Obradovic *et al.*[12] reported that Ni-W alloys exhibit enhanced properties such as corrosion resistance, wear resistance, and catalytic activity for H_2, useful in practical applications.

X-ray diffraction studies conducted by Frantsevich-Zabludovskaya *et al.*[13] indicated homogeneity, ascribable to a solid solution of W in Ni, in spite of the fact that some layered structure was observed in the deposit microstructure.

Tungsten and its alloys are of interest in both theoretical and applied aspects for their specific tribological, magnetic, electrical and electro-erosion properties; and may compete even with ceramics and graphite by virtue of high thermal resistance.[14] They could also be used for magnetic heads, bearings, magnetic relays, catalysis of the processes of oxygen- and carbon containing components of tungsten, electrodes for hydrogen energetics, etc. Studies have shown that Ni-W when used as an electrode material accelerates hydrogen evolution from alkaline solutions.[15] Tungstate alloys with iron group elements are of interest in scientific and industrial applications in compositionally modulated multilayers (CMM) because, when these alloys could have altered magnetic properties for high speed and high density magnetic recording.[14]

2.2 Plating Parameters

Literature cites the influence of various plating variables on the electrodeposition of Ni-W alloys such as, concentration of metals in electrolyte, pH, temperature, current density, stress reducers and complexing agents. These studies are all based on unrecessed electrode experiments.

Brenner[6] compared the tungsten alloy plating baths with respect to the concentration of iron group element, ammonia and complexing agents, pH, current density and temperature of the plating bath. The baths reported by Brenner contained higher concentration of iron group elements than those of other investigator's. Baths

containing ammonia were found to be satisfactory than others with respect to the quality of the deposit and ease of operating the bath. All the alkaline baths reported were operated at a pH ranging from 7 to 10. The current densities used by them ranged from 2 to 5 amp/dm^2 (20-50 mA/cm^2), as cathodic current efficiencies were high in this region.

Brenner's review concluded the following. There is an upper limit to the amount of tungsten in the alloy. The upper limit depends on the codepositing element. For Ni-W the upper limit has been reported to be around 30 wt %. Recently Younes and Gileadi[10] have been able to codeposit up to 76 wt % W in a Ni-W alloy by eliminating ammonia from typical Ni-W plating baths. Under certain conditions, tungsten deposits preferentially, i.e. its percentage in the deposit is larger than its metal percentage in the electrolyte. Tungsten alloys usually electrodeposit at potentials more positive than those at which the iron group metals deposit. The metals in the alloy are intimately mixed, forming either a solid solution or an amorphous mixture, which yields no x-ray diffraction pattern.

Vaaler and Holt[9] studied the deposition of tungsten from an aqueous sulfate ammoniacal citrate bath. They reported a bath consisting of 20 g/l of nickel sulfate 50 g/l of sodium tungstate, 66 g/l of citric acid with a pH of 7 and at a high temperature of 70 °C for obtaining a high percentage of tungsten in the deposit. They were able to obtain bright, shiny nickel-tungsten alloys from the ammoniacal citrate bath with quite satisfactory current efficiencies. They concluded that higher current efficiencies could be attained by increasing the temperature and the nickel concentration of the bath. However, higher nickel electrolyte concentration sacrificed the high W content in the deposit. They also concluded that the ammonia content of the bath is very important in order to maintain higher W content in the alloy, in contrast to Younes and Gileadi's[10] findings. Varying the tungstate concentration lead to different effects depending on citrate concentration. An increase in tungstate concentration with 66 g/l of citric acid had a negligible effect on current efficiency, but with 132 g/l of citric acid caused the current efficiency to decrease. Vaaler and Holt said that this could be due to the decrease in the concentration of simple ions resulting from greater complex formation. The effect was most noticeable at lower current densities. The tungsten content of the alloy increased with the tungstate concentration of the electrolyte. Increases in current density did not produce significant changes in the W content of the alloy. Vaaler and Holt suggested that the bath contained Ni^{2+}, NH_4^+, Na^+, H^+, SO_4^{2-}, WO_4^{2+}, OH^-, $C_6H_5O_7^{2-}$ and other complex ions such as a nickel-citrate anion complex, a nickel ammoniate cation complex and a nickel tungstate complex.

Atannasov *et a*l.[14] discussed the influence of various parameters like cathodic current density, temperature, pH, etc. on alloy composition and current efficiency. They studied a bath with 16.5 g/l of nickel sulfate, 90 g/l of sodium citrate, 30 g/l of sodium tungstate and reported that the W content in the alloy has a linear dependence on current density under complete agitation. They achieved a maximum W content (41 wt %) in the deposit at moderate current densities under no agitation. They concluded that W content in the deposit increased with temperature and strongly depended on the pH. Their results indicate that W concentration in the alloy is higher at a pH of 7 in the absence of stirring. However, at 800 rpm W concentration increased with pH in the range 4 to 8. Microhardness of the deposit was lower in the unstirred solutions.

Bratoeva and Atanassov[8] further investigated the deposition of Ni-W from a sulfamate electrolyte. The process of Ni-W alloy electrodeposition was accompanied by hydrogen evolution, which intensified after –800 mV. The alloy current efficiency decreased with an increase in the cathodic current density. The great amount of hydrogen was correlated with a decrease in tungsten content, which prevented further inclusion of tungsten. An increase in the temperature of the electrolyte lead to the inclusion of more tungsten. They said that the higher temperature facilitates tungsten deposition because of the decrease of the kinematic viscosity of the electrolyte, favoring transport to the cathodic surface. They determined that the process of alloy formation, in comparison with individual nickel deposition, was shifted with the potential of electrodeposition in the positive direction.

Obradovic *et al.*[12] used a bath consisting of nickel sulfate 0.075 M, sodium tungstate 0.2M, citric acid 0.3M, with pH 8.6 adjusted with ammonium hydroxide to deposit nickel-tungsten alloys. They observed a quasi steady state behavior when they conducted a polarization study with a very low sweep rate of 1mV/s. They did not notice any Ni deposit until a potential of –1.31 V vs. SCE was reached. The recorded current was only due to hydrogen evolution. Their analyses showed that deposition of W has a catalytic effect on the Ni deposition as well.

Work done by Podlaha and Landolt[16] on the codeposition of Ni-Mo presented a predictive deposition model, which is also relevant to the Ni-W system. Their mechanism assumed that molybdenum is deposited from an adsorbed intermediate species $[NiCitMoO_2]_{ads}$ releasing ionized Ni species in the process. They explained that Ni reduction also occurs simultaneously but independently of Mo reduction and thus the composition of the alloy depends on the relative kinetics of these two reactions. Obradavic *et al.*[12] suggested that the mechanism of Ni-W deposition is much along the lines of that proposed by the Podlaha and Landolt model for the Ni-Mo system.

Younes, *et al.*[10] achieved 50 atom % (76 wt % W) in the deposit when they used a bath with high tungstate concentration in the absence of ammonia, which is the highest reported concentration of W in a NiW alloy to date. They reported that the increase of tungsten in the deposit with increasing temperature is an artifact, associated with the loss of ammonia. An increase in concentration of ammonia decreased the concentration of the tertiary complex leading to a decrease in the relative amount of W in the plated alloy. Thus, they concluded that the concentration of W in the alloy was higher in the absence of ammonium hydroxide than in its presence. The strong dependence of the alloy composition on temperature, observed in solutions containing ammonia, disappears almost completely in its absence.

Younes *et al.*[10] explained the high Ni/W ratio in the alloy on the basis of parallel reactions occurring during deposition. Ni could either be deposited from its complex with ammonia or citrate and from a complex with W. Though a heterogeneous alloy could be expected, XRD analysis has not supported this suspicion. They explained that the observation of equal amounts of Ni and W in the alloy might be regarded as evidence, for the existence of a tertiary nickel-tungstate-citrate complex.

Maruthi *et al.*[17] studied the effects of various plating variables on a Co-W alloy system in the presence of two complexing agents diammonium hydrogen citrate (DAHC) and dimethyl sulfoxide (DMSO). They noticed preferential deposition of W over Co from a bath containing low W, at a current density of 0.5 A/dm^2 (5 mA/cm^2), temperature of 50

°C, pH of 7.5, and 0.05 M of DAHC and DMSO. An increase in current density increased deposition of W. They also found that W content in the deposit increased slightly with an increase in DMSO concentration, while W content decreased with an increase in the concentration of DAHC. They concluded that DMSO acts as a complexing agent while it is also absorbed on the cathode surface and stimulates the electrochemical discharge reaction, which aids in the codeposition of W.

In the study of ternary alloys consisting of W, Singh, *et al*[11] found that W content in a Ni-W-Co deposit increased with an increase in pH, temperature and current density. The metal content in the deposit was promoted by an increase of its metal ion concentration. Also, it was found that, at lower concentrations, when the concentration of W in the bath was increased, its content in the deposit was higher than that in the bath. Hydrogen evolution was found to increase with the tungsten content in the bath. They reported an optimum bath concentration consisting of nickel sulfate 0.108M, sodium tungstate 0.0045M, citric acid 0.333M, and sodium chloride 0.17M. Fine grained, bright and adherent deposits were obtained near current densities of 15 mA/cm^2, between pH 4.5 and 6.0, and up to 35 ºC. Tungsten content in the deposit was said to increase with temperature.

Singh *et al.*[11] also investigated the various factors responsible for codeposition of reluctant metals. They found that a large activation polarization, a discharge potential in the vicinity of the equilibrium potential of the reluctant metal, and ability to form a solid solutions are the factors responsible for codeposition of the reluctant metal with other metals.

Hubbard[18] showed that the NiMo mechanism proposed by Podlaha and Landolt[16] is also consistent with two different Ni-W citrate electrolytes, one with an excess of Ni and another with an excess of W. It was also noted that at high overpotentials both the Ni and W reaction rates were inhibited by the side reaction. Hubbard[18] made the first attempt of plating NiW alloys into deep recesses of 500 microns. While successful, the deposit contained cracks and voids. He observed a lower concentration of W in the recess compared to unrecessed cylinder electrodes, plated under similar conditions.

2.3 Deep Recess Plating

Electroplating into recesses patterned in a resist was first evolved at the IBM T.J. Watson Research Center as through mask electroplating, which is now known as LIGA technology. Cu is the first material that was electroplated into patterned resists by Romankiw and his co-workers.[3] He also discussed that the important problems in through mask electroplating are current distribution and mass transport, particularly when convection doesn't reach deep into narrow patterns. Mass transport limitations result in a depletion in the supply of metal ions at the electrode surface, which lowers the reaction rate and also results in the accumulation of reaction products and hydrogen bubbles. He discussed that current distribution and plating thickness uniformity depends on the size of features plated, the separation of features from each other and the formulation of electrolyte. He also said that, as the depth to width aspect ratio increases, the plating process into the deep recesses becomes primarily diffusion controlled, until the deposit nears the top of the recess.

Ehrfeld *et al.*[4] discussed microelectroplating materials for LIGA technology citing the specific applications of different materials. They have listed Ni, Cu, and Ni-Co as standard materials for mold insert applications. Testing and developing Co-W and Ni-W were reported for obtaining hard microstructures. A Ni-W part, ~25 μm thick and which has a hardness of 600 HV at a W concentration of 10% was shown as a part of planetary gear system. Au, Ag, Fe, Pd, and Ni-Fe were among the other materials used by them in the LIGA electroplating step.

Kupper *et al.*[19] explained the various problems associated with cathodic alloy deposition in microstructures. They indicated that crucial problems arise from the concentration distribution, the resulting composition of the alloy, the occurrence of side reactions and the influence of convection. They generalized that, concentration distribution in a microstructure is a problem associated with diffusion controlled metal deposition and a non-uniform concentration distribution could result in preferential growth in certain areas. Also, composition of the alloy could be disturbed due to this. They also noted that side reactions could occur more frequently due to a less effective transport of metal ions and that local pH rises could result in a shift of complexation equilibria as well. They discussed that convection could not be a remedy to this problem because microcavities are convective hindrances.

Bond *et al.*[20] compared the chronoamperometric response at inlaid and recessed disc microelectrodes experimentally and theoretically. They showed that all microelectrodes when operated at concentration polarized conditions in the steady state, have the same "iR drop" regardless of geometry and that a recessed microdisc electrode would achieve a steady state regardless of solution agitation outside the recess. They modeled the concentration changes with time and showed that the steady state current at a recessed disc electrode is smaller than that of the inlaid disc electrode by the factor $(4L/\pi a) + 1$ where `L` is the depth of the recess and `a` is the radius of the disc. The time necessary to reach steady state was determined by solving the following system of equations:

$$\frac{\partial c}{\partial t} = D \frac{\partial^2 c}{\partial x^2} \qquad \text{[Fick's second law]} \quad ....(1)$$

$$c = c^b, \ x = L \quad ....(2)$$

$$c = 0, \quad x = 0 \text{ all } t > 0 \quad ....(3)$$

$$c = c^b, \text{ all } x \geq 0, t = 0 \quad ....(4)$$

The concentration gradient at the electrode surface was obtained by solving equation (1) through (4). The current was obtained from Fick's first and Faraday's laws as

$$i = \pi nFDa^2 \left(\frac{\partial c}{\partial x} \right)_{x=0} \quad ....(5)$$

Substituting for concentration gradient in equation (5) yielded the steady state current as $i = \{ \pi nFc^bDa^2 / L \} \{ 1 + 2 \exp(-\pi^2Dt / L^2) + 2 \exp (-4\pi^2Dt / L^2) + \ldots\}$

The time required for the current to come within 5 % of its steady state value was found to be $\{(4L + \pi a)^2 \ln(38)\} / (16\pi^2D)$. This expression was used to estimate the order of magnitude for the pulse length used in this study.

In this thesis pulse plating is to be considered because pH rises are expected in the recesses. Pulse electrolysis is a common practice in electrodeposition for thin films.[21]

Theoretical aspects have been reviewed by IBL.[22] Related to thin films on unrecessed surfaces two important features of pulse electrolysis are: 1) the ability to generate high instantaneous current densities and hence very high negative potentials which could cause a shift in the ratio of reaction rates with different kinetics and 2) the influence of "off time" during which adsorption and desorption phenomena as well as recrystallization of the deposit could occur. It is the second factor, which is important to the work presented in this thesis. The "off time" is necessary for diffusion of reaction products that adversely affect the electrodeposition reaction. In addition, very rough or powdery deposits are obtained when the solution in the immediate vicinity of the cathode is strongly depleted of metal ions. Therefore, surface morphology may also be dependent on the pulse conditions.

CHAPTER 3. STATEMENT OF PURPOSE

The primary objective of this study is to demonstrate that it is possible to electrodeposit Ni-W alloys into 500 μm recesses for MEMS applications by developing necessary plating methodologies. To date, no study has demonstrated deposition of Ni-W in recesses greater than 50 μm. The secondary objective is to be able to control the composition of the alloy in the microstructure.

There are various applications of Ni-W alloys, especially in the MEMS industry, due to its excellent mechanical, corrosion resistant and tribological properties. Whereas a lot of work has been reported concerning plating Ni-W alloys on planar surfaces, very little has been reported on plating into deep recesses, despite its potential applicability in the MEMS industry.

Prior work in our laboratory at Louisiana State University[18] with unrecessed electrodes indicated a citrate bath at 70 °C and pH 10 could yield a reasonable amount of tungsten (> 8 wt %) in the deposit with a high current efficiency. Hence, citrate based electrolytes have been examined here.

Problems with gas evolution and pH rises at the electrode surface involved in plating into deep recesses especially with Ni-W were identified. Pulsing schemes with large relaxation times were used to remedy these problems. Different pulsing conditions were tried to optimize the processing time and control composition variance in the deposit. The applicability of the different plating schemes developed was also tested on other alloy systems.

CHAPTER 4. EXPERIMENTAL

4.1 Electrolytes Used

Two types of electrolytes, sulfamate and ammoniacal citrate, were studied. Sulfamate bath was adapted from Atanassov *et al*.[14] It consisted of nickel sulfamate, sodium citrate and sodium tungstate. This bath was examined due to the high tungsten weight percents reported. The ammoniacal citrate bath was adopted from Hubbard.[18] Ammoniacal citrate baths, with varying concentrations of sodium citrate, nickel sulfate and sodium tungstate, were chosen to investigate the applicability of the baths for microstructure development. Ammonium hydroxide was added to obtain a constant pH =10 at 70 °C and pH was measured using Orion® Model 420A pH meter.

The compositions of the baths considered are listed in Table 4.1. Equimolar bath (Bath #1) contained equal concentrations of sodium tungstate and nickel sulfate. Double Tungsten bath (Bath #2) contained double the concentration of sodium tungstate present in Bath #1, remaining concentrations held constant. Low Ni bath (Bath #3) contained low Ni concentration than in Bath #1 and Bath #2. The ratio of nickel sulfate and sodium citrate concentrations was held constant in all the baths considered. Intermediate bath (Bath #4) contained more Ni concentration than in Bath #3 but low Ni concentration than in Bath #1 and Bath #2.

Table 4.1 Compositions of ammoniacal citrate baths used

Equimolar bath (Bath #1):	**Concentration / M**
Sodium Citrate	0.5
Sodium Tungstate	0.4
Nickel Sulfate	0.4
Double Tungsten bath (Bath #2):	
Sodium citrate	0.5
Sodium Tungstate	0.8
Nickel Sulfate	0.4
Low Ni bath (Bath #3):	
Sodium citrate	0.125
Sodium Tungstate	0.4
Nickel Sulfate	0.1
Intermediate bath (Bath #4):	
Sodium citrate	0.25
Sodium Tungstate	0.4
Nickel Sulfate	0.2

4.2 Substrate Preparation

The substrate for deep recess electrodeposition consists of four different layers, which are Cu, CuO, layer of bonding solution, and polymethylmethacrylate (PMMA). Each step in the process of substrate preparation is described below. A square copper plate 5 cm × 5 cm × 0.08 cm was used as a substrate (cathode). It was pretreated by washing with soap, soaking in 10% H_2SO_4 for 2 minutes and then degreasing by rinsing in acetone. The copper plates were oxidized in *Cu- oxidizing* solution at 95° C until a uniform black oxide layer was formed on the copper plate. The composition of the solution is listed in Table 4.2. Subsequently, it was placed in water and dried in air.

A 500 μm thick PMMA photoresist, which is of the size of the copper substrate, was adhered onto the copper substrate by using a *bonding* solution, see Table 4.2. The substrate was then subjected to a uniform pressure of about 2 Psi.

The prepared substrate was sent to the Center for Advanced Microstructures and Devices for x- ray lithography. Figure 4.1 shows a schematic of the substrate preparation. The photoresist was patterned by exposure to x-ray radiation through a mask having the desired pattern at the Center for Advanced Micro Devices (CAMD). The mask is a glass or quartz plate with a gold pattern, transparent in some regions and opaque where covered with gold. Since PMMA is a positive photoresist, the radiation causes chain scission of the exposed part of the resist enabling it to dissolve in a developing solution. The exposure parameters used at CAMD for the two different masks used are given in Table 4.3.

The exposed regions were dissolved away by developing using a *developer* solution, *pre-rinse* and *rinse* solutions. Their compositions are given in Table 4.2. The developing process consisted of four cycles of sonication, each consisting of developing in *developer* solution for 10 min, rinsing in *pre-rinse* solution, which is an old rinse solution for 2 min, and rinsing in *rinse* solution for 1 hr. The substrate was then etched in *CuO-etch* solution for 2 min or until the copper oxide is completely removed. The constituents of the etch solution is also provided in Table 4.2. Thus, the holes or squares are open to the copper substrate creating a deep recess for electrodeposition. The final substrate was used as a Deep Recess Electrode (DRE).

Copper cylinder electrodes with 1 cm diameter and 1.2 cm height were used as substrates for RCE experiments. They were pretreated before deposition in the following manner. They were polished using 600 and 1500 grit papers in sequence, rinsed in 10% sulfuric acid for removal of any oxides using a 1510 Bransonic® ultrasonic bath cleaner and then degreased using acetone.

4.3 Cell Design and Operation

The Deep Recess Electrode (DRE) was placed into a jig to hold it in place during electrodeposition. The jig has two cylindrical disks, which are held together using screws. The bottom disk has a copper plate recessed to seat the copper substrate. A copper wire soldered to the bottom of the recessed plate served as the cathode connection. The top disk has an opening that enables the electrolyte solution to reach the substrate. The thickness of the disk opening, which is a recess for the substrate helps in rendering a

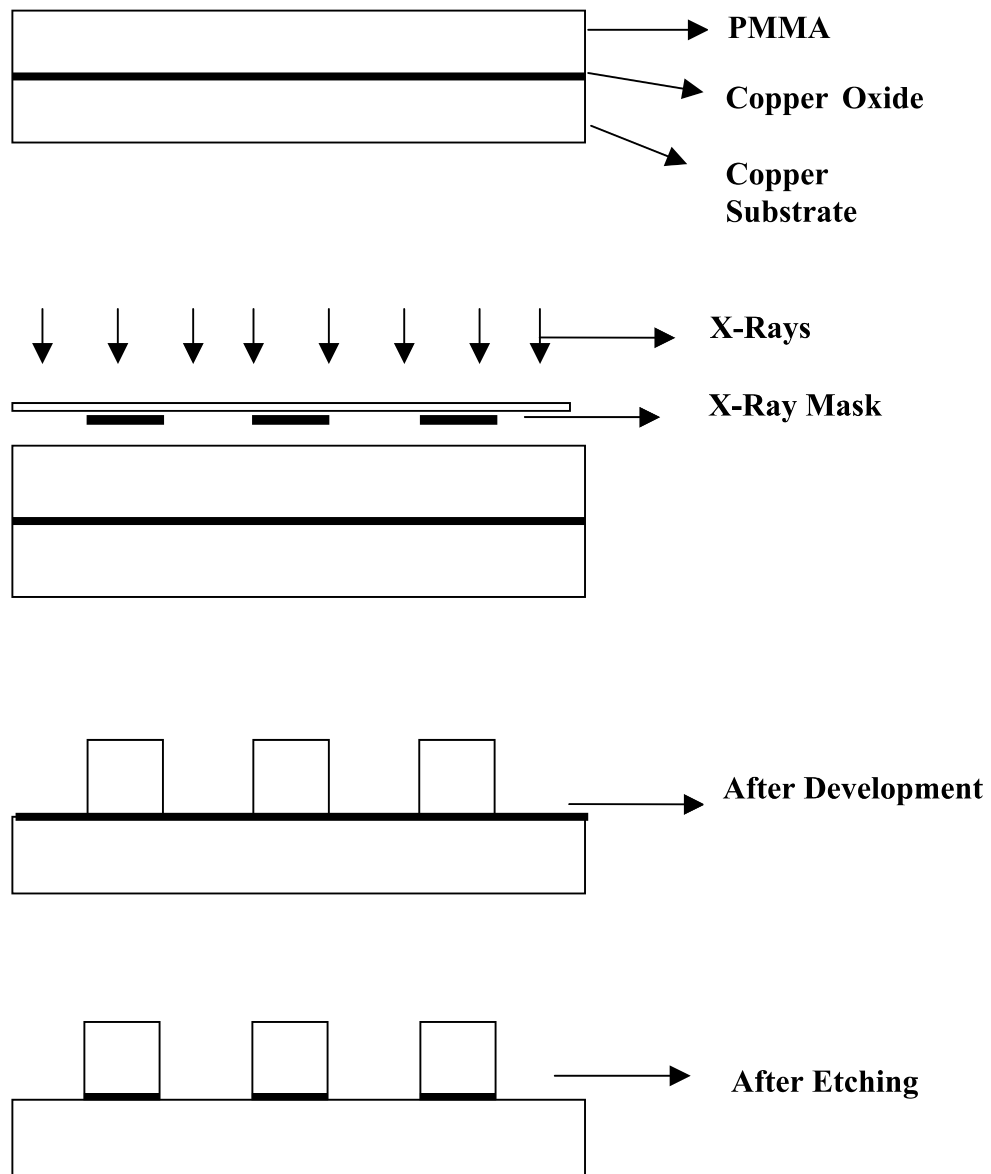

Figure 4.1 Schematic of recessed substrate preparation with x-ray exposure at CAMD

Table 4.2 Recipes of solutions used during substrate preparation

Copper oxidizing solution		Bonding solution	
$NaClO_2$	54.26 g/l	MethylMethacrylate	17 g
NaOH	68.00 g/l	Powdered PMMA	1 g
Na_2CO_3	11.44 g/l	Benzoyl Peroxide	0.3 g
NaCl	4.67 g/l	Dimethyl aniline	0.2 g
Developer solution		**Rinse solution**	
Diethylene glycol butyl ether	600 ml	Diethylene glycol butyl ether	800 ml
Morpholine	200 ml	Water	200 ml
2-minoethanol	50 ml		
water	150 ml		
Copper oxide etch solution			
Potassium chloride	0.5 M		
Hydrochloric acid	0.5 M		

Table 4.3 Exposure parameters used by CAMD

Parameter	Quantity
Ring Energy	1.3 GeV
Filter	14 μm Al
He Pressure	25 torr
Scan Length	0.4 inches
Dose at the counter	9100 mA.min
Bottom Dose	3500 joules/cm^3

uniform current distribution to the substrate. The cathode was seated on the recessed plate and the two cylindrical disks are fastened together with screws. A Ni sheet placed approximately 1 inch above the jig served as the anode. A saturated calomel electrode was used as a reference electrode. A stir bar was used to provide bulk mixing.

In order to make sure that there is no oxide left in the holes, a 10% H_2SO_4 was forced into the holes using a Nucerite® Nalge / Sybron corporation water vacuum. The holes were thoroughly cleaned with water and then the electrolyte was forced down into the holes using vacuum to ensure that it reached the copper substrate. The cell was sealed to harness any evaporation of ammonium hydroxide or electrolyte. The cell assembly was

then lowered into a hot water bath maintained at 70 °C using a Fisher Scientific isotemp® Model 2100 water pump heater. A schematic of the cell used is shown in Figure 4.2.

Figure 4.3 shows a schematic of the experimental cell used for electrodeposition onto RRCE with anode (platinum mesh), cathode (RRCE) and reference electrode (saturated calomel electrode). An RRCE was chosen in order to investigate the influence of mass transport boundary layer thickness on the deposit. It further allows us to estimate the limiting current for deep recessed electrodes. Also, it helps in attaining a uniform primary current distribution along the length of the electrode resulting in uniform thickness and composition.[23]

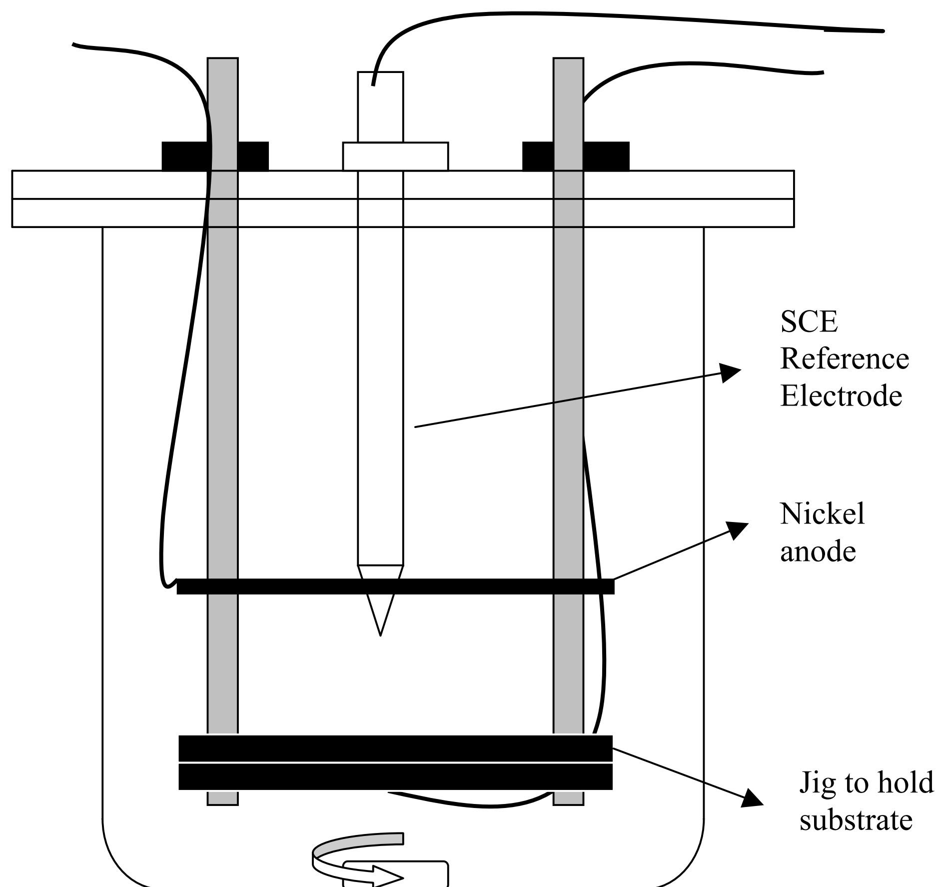

Figure 4.2 Schematic of the cell used for deep recess plating

A Pine instrument company Analytical Rotator Model AFMSRX was used to operate RCE at different rotation rates. A platinum plated titanium mesh was used as the counter electrode and a saturated calomel electrode (SCE) was used as the reference electrode.

4.4 Experimental Procedure

Deep recess plating was accomoplished using pulse plating techniques. Pulse plating was carried out using an EG&G Princeton Applied Research

Potentiostat/Galvanostat, Model 363 and an EG&G Parc Universal Programmer Model function generator. Microposts were deposited either by potentiostatic or galvanostatic pulsing. A schematic of the pulsing scheme is shown in Figure 4.4.

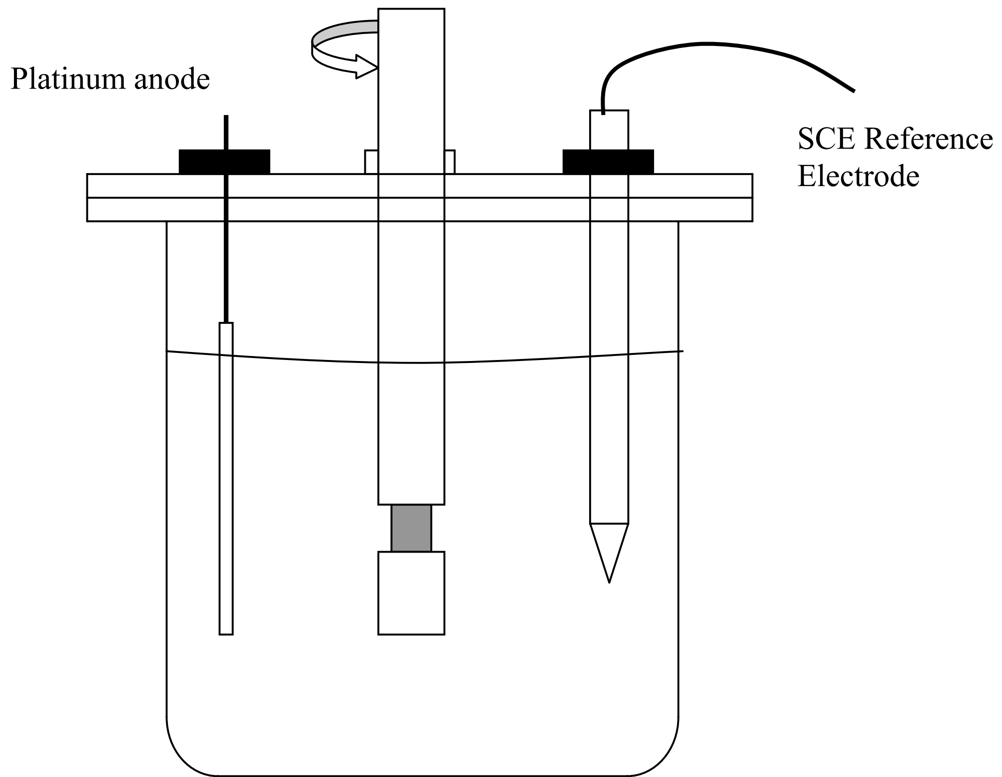

Figure 4.3 Schematic of the cell with RCE, platinum anode, and SCE reference electrode.

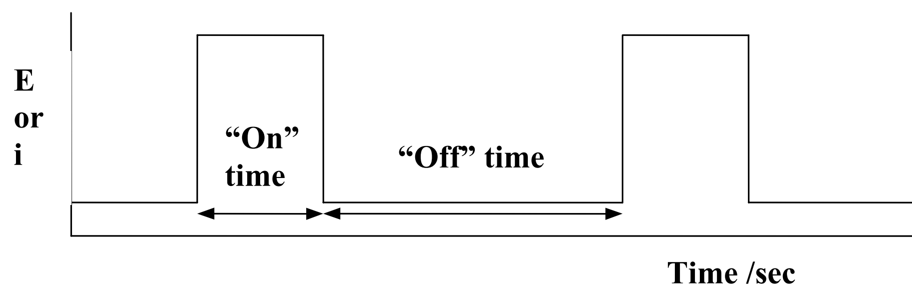

Figure 4.4 A schematic of the pulsing scheme for deep recess electrodeposition.

Each pulse consisted of an "On" time during which potential or current was applied, and an "Off" time during which an open circuit potential or zero current was applied.

Electroplating on the RCE, was carried out with currents up to -1 A using an IM6e Zahner® Impedance Measurement/Potentiostat/Galvanostat system. All experiments were carried out at atmospheric pressure and at 70° C. A precision® 180 series water bath was used to maintain the operating temperature.

Different current densities, with constant current density for a deposition time of 30 minutes or a constant charge density of 27000 C/cm^2, were applied to plate Ni-W onto RRCE. The potentials measured during deposition and those recorded during polarization studies were corrected for ohmic drop using a Zahner® Electrochemical Impedance Spectroscopy (EIS) system. A Mettler® model AE240 five decimal place weight balance was used to weigh the samples before and after electrodeposition.

Polarization curves were obtained using Linear Sweep Voltammetry. A IM6e Zahner® Impedance Measurement/Potentiostat/Galvanostat system was used to produce polarization scans. Different scan rates of 2 V/s, 5 mV/s and 10 mV/s were chosen to match different rotation rates and concentrations of the electrolytes.

Composition along the length of the deposits, current efficiencies, and partial current densities of Ni and W were calculated in order to interpret the applicability of the baths to develop microstructures.

Composition analysis of the deposits on the copper cylinders was done by using Kevex Omicron x-ray Fluorescence Spectroscope. The partial current densities of Ni (i_{Ni}) and W (i_W) are the amounts of current contributing to that specific reduction reaction, while the rest is side reactions including the H_2 evolution.
The partial current densities, i_{Ni} and i_W are defined as,

$$i_{Ni} = \frac{(-1000)(M_{total})(x_{Ni})(n_{Ni})(F)}{(60)(MW_{Ni})(t)(A)} \quad [=]\ mA/cm^2$$

$$i_W = \frac{(-1000)(M_{total})(x_w)(n_w)(F)}{(60)(MW_w)(t)(A)} \quad [=]\ mA/cm^2$$

where M_{total} is the total deposited mass of alloy in grams, x_{Ni} and x_W are the weight fractions of Ni and W, n_{Ni} and n_W are the number of electrons needed to reduce Ni and W (2 and 6), F is Faraday's constant (96485 C/eq), MW_{Ni} and MW_W are the molecular weights of Ni and W, t is the total plating time and A is the area of the electrode (A=3.77 cm^2).
Side partial current densities are defined as,
$i_{side} = i_{total} - (i_{Ni} + i_W)$ [=] mA/cm^2
and current efficiency is defined as

$$\varepsilon\ \% = \frac{((i_{Ni} + i_W)}{i_{total}} \times 100.$$

where i_{total} is the total applied current density.

4.5 Deposit Analysis

After the deposition into the recesses was completed, the sample was polished to remove any overplate and placed in acetone to dissolve away the PMMA. A part of this sample was cut using a diamond saw and mounted in epoxy in a way that the length of the post is available for inspection. The cast was polished using 500 and 1500 grit papers, and then micropolished using microgrit papers, diamond and aluminium oxide pastes in order to obtain a 0.3 micron finishing. The posts were then analyzed using a Superprobe 733-electron microprobe (JEOL company) with wavelength dispersive x-ray spectrometer for chemical composition of Ni and W along the length of the micropost. The morphology of the deposits was obtained from a Scanning Electron Microscope (SEM) (Joel JSM-840A).

In electron microscopy, a sample is bombarded with a finely focused beam of monochromatic electrons from an electron gun. The incident electron beam interacts with the top layers of the sample and the products of this interaction follow trajectories away from the surface. Products from the interaction of the incident electron beam with the sample are detected. It is the secondary electrons that are detected with the electron being scanned across the sample surface.

Another product of the surface interaction with the incident electron beam is X-ray photons that have wavelengths and energies dependent upon element identity and on the electron shell causing the emission. By analyzing the X-ray photons, a local chemical analysis of the surface can be conducted. This is the principle used by an electron microprobe. X-rays generated can be measured and characterized by two types of X-ray spectrometers. The first type is a wavelength dispersive spectrometer (WDS). Using WDS the wavelength is scanned, and the wavelengths corresponding to the ejected photons are determined by using diffraction from crystals mounted in the spectrometer and manipulating the angle between the crystal and the photon beam. A second type is an energy dispersive spectrometer (EDS) in which a multi channel analyses gives the photon energy spectrum. In both cases, peaks are assigned to particular elements and their areas to the percentage of the element present.[24] The measurements are processed, calculated and corrected to provide a visual or numerical result. WDS provides quantitative chemical analysis that reports down to 0.01 wt% for many elements and this technique was used to quantify the composition of the deposits.

Composition of the deposits on the cylinders was obtained using Kevex Omicron X-ray Fluorescence Spectroscope. Kevex Omicron uses the energy-dispersive x-ray spectrometry (EDS) analytical method to analyze the elements. When an atom is bombarded with high energy x-rays, inner shell electrons may be removed from their atomic shell that results in the filling up of that vacancy by an electron from an outer shell. Each transformation results in the loss of a specific amount of energy, namely the difference in energy between the vacant shell and the shell contributing the electron. This energy, which uniquely identifies the element from which it came, is given up in the form of electromagnetic radiation x-rays. The x-rays are named after the type of the transition involved.

The Omicron spectrometer uses an X-ray source to generate X-rays from the sample, which are detected by a detector. The X-ray source consists of an electron gun and a target sealed inside a vacuum envelope. X-rays are generated by bombarding a

target with either charged particles (electrons or alpha particles) or high-energy photons (x-rays or gamma rays). These emitted x-rays are characteristic of the elements present because of the physical properties of atomic structure. The target is maintained at a high voltage with respect to the electron gun, such that the electron beam generated from the filament is accelerated toward it. The detector absorbs x-rays emitted from the sample and then acts as an energy to charge transducer quickly passing information to an amplifier and multichannel analyzer. The detected X-rays are digitized and sorted and presented as a spectrum, which is plotted from raw X-ray data in counts vs. energy format. These counts are calibrated with known standards so that the composition of the alloy can be determined.

CHAPTER 5. RESULTS AND DISCUSSION

5.1 Choice of Electrolyte

5.1.1 Sulfamate Bath

A sulfamate electrolyte containing 16.5 g/l of nickel sulfamate, 90 g/l of sodium citrate and 30 g/l of sodium tungstate was adopted from Atanassov *et al.*[14] Electrodeposition onto cylinders rotating at 300 rpm was carried out at 60 °C and a pH of 7 as they reported higher amounts of tungsten under these conditions. The deposits were analyzed for composition of the alloy along the height of the cylinder, and the average value reported. Figure 5.1 shows the relation between weight % W and the applied current density with the error bars representing the standard deviation in weight percent. A high weight percent W is found at low current densities, which decreases as the applied current density increases. Current efficiencies of the plating process were determined by measuring the weight and composition of the deposits and shown in Figure 5.2. Current efficiencies are all below 40%. Partial current densities are plotted against the potential in Figure 5.3 to show the relation between the reaction rate

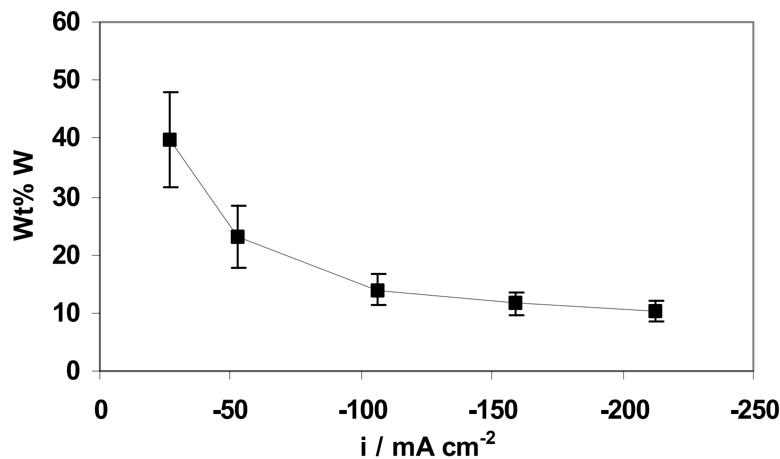

Figure 5.1: Weight percent tungsten against applied current density at 300 rpm for sulfamate bath, pH of 7, at 60 °C

and driving force. The potential was recorded halfway during the plating process. The figure clearly illustrates that huge side reactions accompany the deposition processes. The nickel rate increases more with potential than W, which is consistent with Figure 5.1, having a high W weight % at low current densities. These results are in agreement with literature findings.[14] Under these conditions it would be extremely difficult to plate into deep recesses because the side products would severely hamper the deposition process. Hence this bath was not recommended for deep recess plating.

5.1.2 Citrate Bath

A Ni-W electrolyte having equal concentrations of nickel sulfate and sodium tungstate, adopted from Hubbard's thesis[18], was examined. The deposit composition,

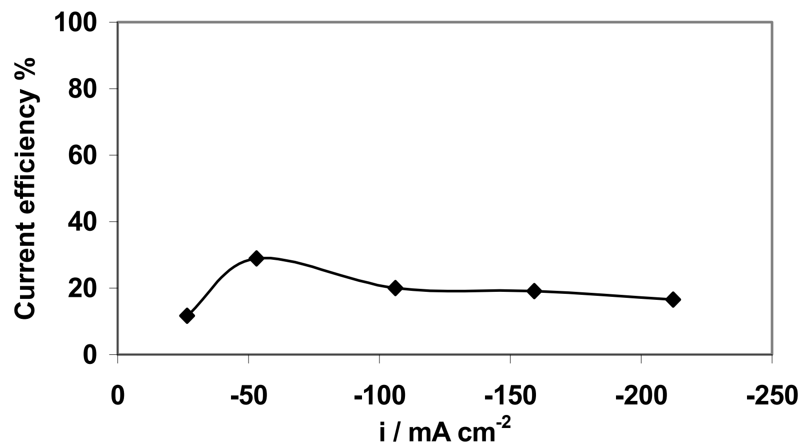

Figure 5.2: Current efficiency vs. applied current density at 300 rpm for sulfamate bath, pH of 7, at 60 °C

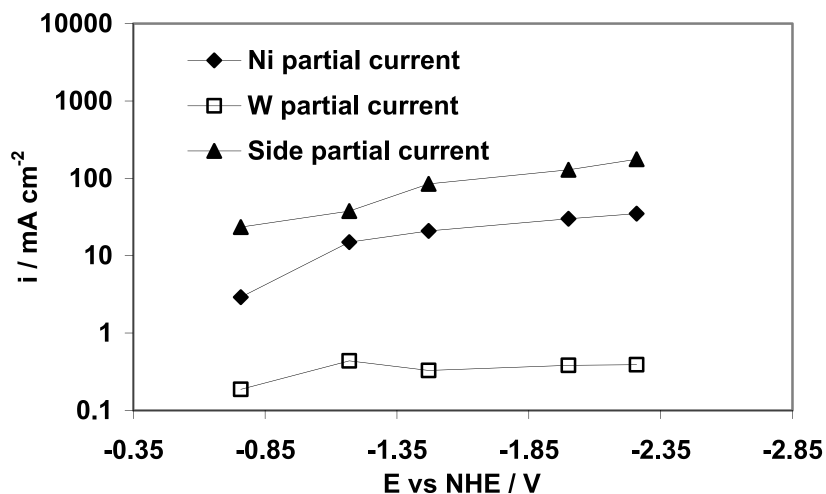

Figure 5.3: Partial current densities of Ni, W and side reaction as a function of potential at 300 rpm for sulfamate bath, pH of 7, at 60 °C

current efficiency and partial currents were determined by conducting experiments on rotating cylinder electrodes at 300 rpm. Figure 5.4 shows the weight percent of tungsten obtained as a function of current density. It was observed that the composition of the alloy did not vary significantly with the current density. The W composition of the deposit is much lower than that obtained from sulfamate bath in Figure 5.1. Current efficiency data in Figure 5.5 shows, however, that current efficiencies close to 100 % could be obtained in the chosen range of current densities, unlike the sulfamate electrolyte in Figure 5.2. Partial currents for Ni, W and side reactions are shown on a semi-log plot in Figure 5.6. The side reaction was observed to be significantly less in this deposition. Thus, it was concluded that a citrate-based bath holds promise for deep recess plating.

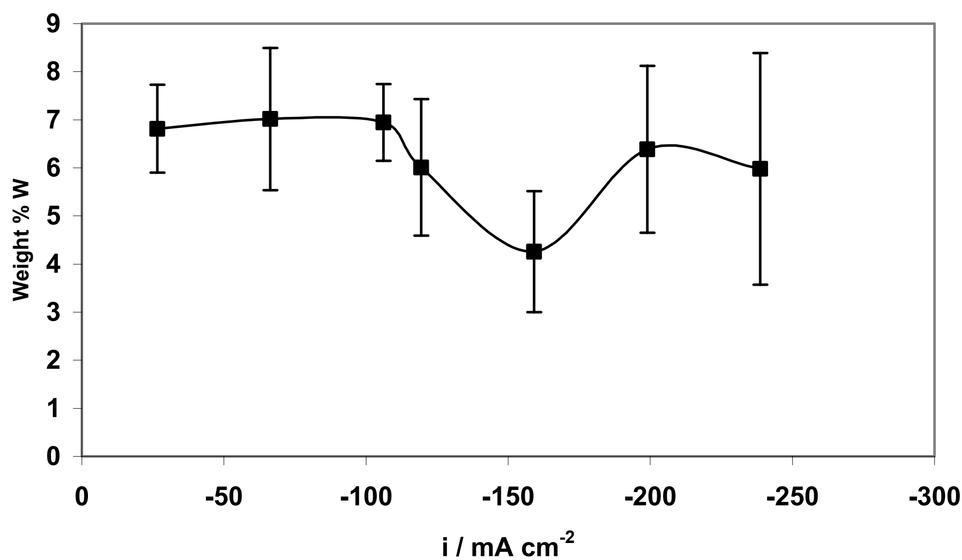

Figure 5.4: Weight Percent W as a function of applied current density for Bath #1 (Equimolar) at 300 rpm, pH of 10, at 70 °C.

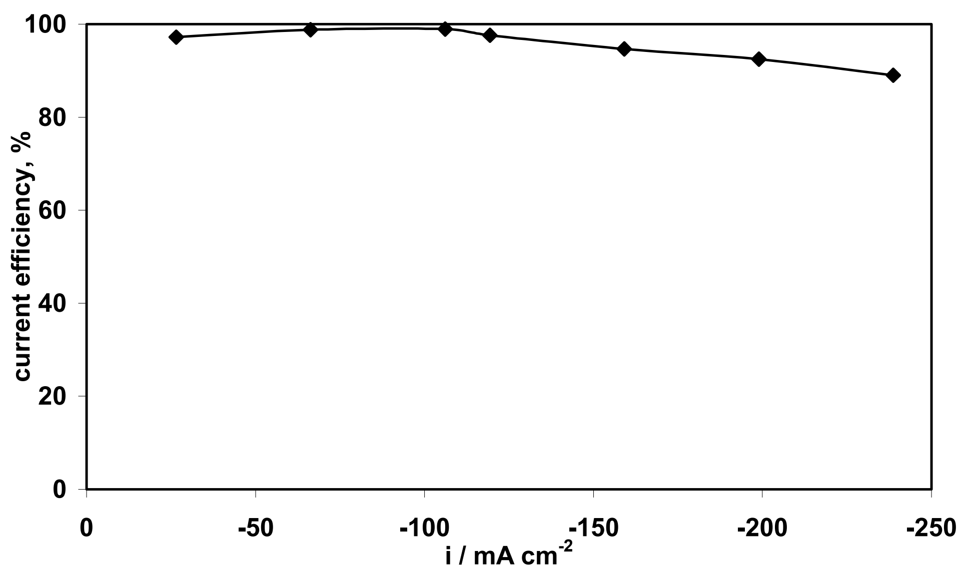

Figure 5.5: Current efficiency as a function of applied current density for Bath #1 (Equimolar) at 300 rpm, pH of 10, at 70 °C.

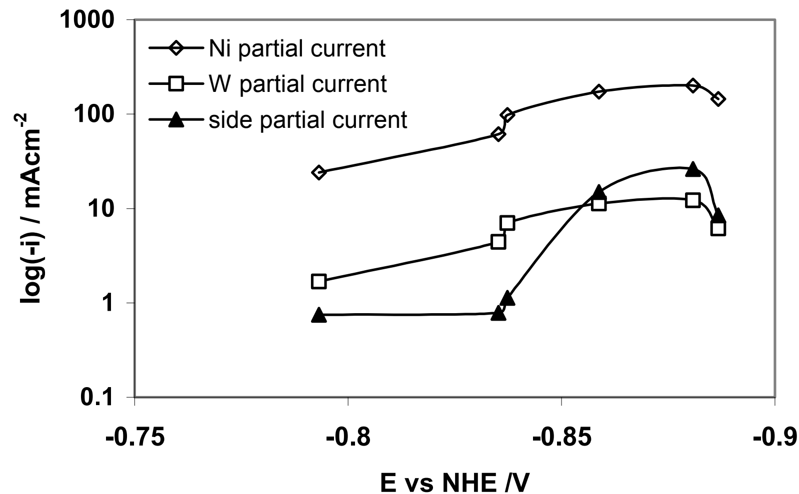

Figure 5.6: Partial current densities of Ni, W, side reactions as a function of potential for Bath #1 (Equimolar) at 300 rpm, pH of 10, at 70 °C.

5.2 Deep Recess Plating

According to the induced codeposition mechanism, evolution of hydrogen and generation of hydroxyl ions are inherent parts of Ni-W alloy electrodeposition. Therefore, bubbles might become incorporated into the deposit causing voids or cling to the surface resulting in non-uniform deposit growth. Also, moderate pH rises could influence the deposition mechanisms, resulting in compositional changes. If the pH rise is severe, undesirable precipitation products could be incorporated in the deposit, sometimes even blocking the surface terminating the deposition. Improving convection is not an answer to this problem because microcavities are convective hindrances. Volume in the recess remains stagnant no matter how vigorous the agitation is in the bulk.

The obvious method to counteract the problems associated with side reactions and side products is to optimize the plating conditions so as to avoid operating conditions where the side reactions occur. However, in systems like Ni-W with large electronegative reduction potentials in aqueous solutions, the side reactions can only be minimized to a certain extent but cannot be completely avoided. RCE experiments on different baths with varying conditions clearly explain this phenomenon. In addition, the hydroxyl ion is generated during the reduction of the tungstate ion.

Attempts at DC plating were not favorable. Precipitation was observed terminating the deposition as expected from large pH rise. This occurred even when the current efficiency was high, not only because of the hydroxyl ion generation from water reduction but from the tungsten reaction itself.

$$WO_4^{-2} + Ni(II) + 4H_2O + 8e^- \longrightarrow W(s) + Ni(s) + 8OH^- \quad \text{………. ………eq (1)}$$

Thus our line of thought takes a different path. Pulse potential and pulse current schemes were implemented to manage the gas evolution reactions and local pH rises. These methodologies are based on using a long relaxation time that allows unwanted reaction products to diffuse out of the recesses and allows metal ions to replenish the electrolyte in the recess. Long relaxation times were chosen by considering the estimated time required for the recess to reach equilibrium while at the limiting current. An estimate of this time was obtained by solving Fick's second law of diffusion for the recess, approximated as: $t \equiv (4H + \pi a)^2 \ln(38) / 16\pi^2 D$. For a boundary layer thickness of 500 microns and a diffusion coefficient of 10^{-5} cm^2/sec the relaxation time is 31.85 sec.

A pulsing scheme with one segment 'On' at an applied current and another segment 'Off' at zero current is shown in Figure 5.7. The deposition time or 'On' time chosen was less than the time required for the surface concentration of reacting species to go to zero, which depends on the pulse current density and diffusional limitations. The relaxation time or 'Off' time chosen was more than the time required for the side products to diffuse back into the bulk solution.

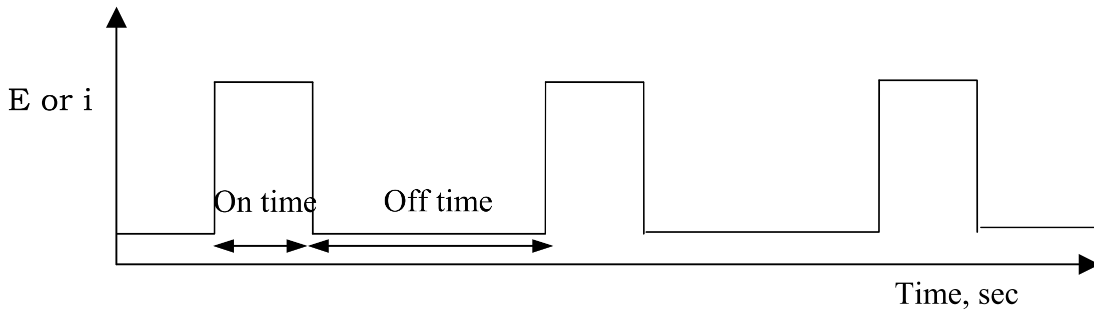

Figure 5.7 Schematic of the pulsing scheme used for deep recess plating

5.2.1 Potentiostatic Pulsing

Electroplating into the recesses was done by potentiostatic pulsing, using Bath #1, Bath #3, and Bath #4, which was not successful. A potential more negative than the open circuit potential was applied during the 'On' time, and the open circuit potential was applied during the 'Off' time. Figures 5.8-10 show the microposts obtained from Bath #3 (low Ni concentration) using this scheme at different 'On' potentials in the range –1.2 V to –1.5 V. An 'On' time of 30 sec and 'Off' time of 60 sec were used for this purpose. Microposts in all the cases began to grow but the deposition terminated eventually. The non-uniform morphology of the deposits shown in these figures is indicative of the side reactions occurring because side reaction would cause bubbles to sit on the surface resulting in preferential deposit growth. Deep recess plating was also done by potentiostatic pulsing using Bath #1 and Bath #3. Pulsing potential of –1.2 V with 30 sec 'On' time and 60 sec 'Off' time were used. Deposits were grown preferentially in certain areas resulting in mushroomed posts. No single experiment resulted in uniform growth of the deposits. Also, the posts suffered from poor adhesion to the substrate. Figures 5.11 shows the overplated posts and sites where posts were broken, illustrating these problems. There are several reasons behind the failure of this plating scheme the major

one being the lack of control this scheme has, over the deposition process. This was evident from the large cathodic and anodic decays at the beginning and end of each potential step. Also, the ohmic drop decreases with the growth of the deposit making the applied potential more positive. The open circuit potential was also changing which is a function of the deposit composition and solution surface concentration. Hence, the open circuit potential needs to be adjusted by measuring the current which results in a zero value.

The original impetus of conducting a pulsed potentiostatic scheme has the advantage of a high deposition rate. This is because higher limiting currents occur as the boundary layer thickness decreases with the deposit growth as was also noticed during the deposition process.

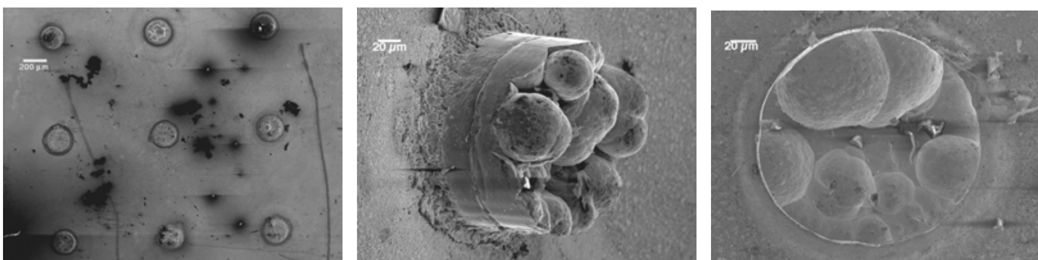

Figure 5.8: SEM micrograph of Ni-W microposts obtained by potentiostatic pulsing from Bath #3, pH of 10, at 70 °C. 'On' potential: -1.15 V vs. SCE 'Off' potential: open circuit

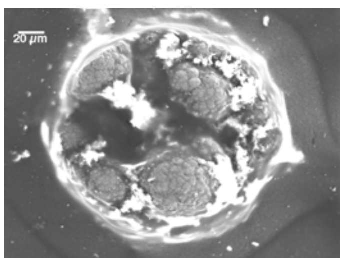

Figure 5.9: SEM Micrograph of Ni-W microposts obtained by potentiostatic pulsing from Bath #3, pH of 10, at 70 °C. 'On' potential: -1.25 V vs. SCE

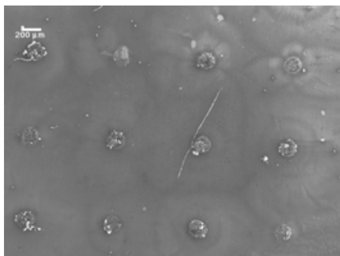

Figure 5.10: SEM micrograph of Ni-W microposts obtained by potentiostatic pulsing from Bath #3, pH of 10, at 70 °C. 'On' potential: -1.3 V vs. SCE

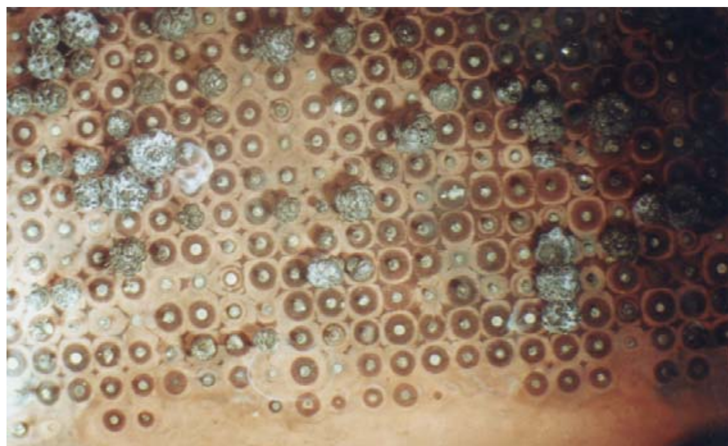

Figure 5.11: Optical picture of the Ni-W microposts deposited from Bath #4 by potentiostatic pulsing with pulse potential of –1.2 V, 'on' time of 30 sec and off time of '60' sec.

5.2.2 Constant Current Pulsing

The failure of the potentiostatic pulsing scheme lead to the use of a galvanostatic pulsing scheme. Deposition currents were chosen so that they lied in the kinetic region and not in the mass-transport region in order to avoid transport limitations in an attempt to control the deposit composition.

Galvanostatic pulsing with a pulse current of 16.5 mA/cm^2 and a duty cycle of 0.2 resulted in successful plating of Ni-W microposts from Bath #4. Figures 5.12 and 5.13 show the optical and SEM pictures of the microposts thus obtained. The 'On' and 'Off' times were kept at 15 and 60 sec respectively. At the end of three days, 200 μm tall microposts were observed. The average growth rate was, 67 μm / day.

This experiment was repeated on a substrate with a square mesh pattern with a slightly higher current density of 17.5 mA/cm^2 and a duty cycle of 0.25. Figure 5.14 shows the microposts grown half way by this scheme .The 'On' time of 15 seconds and 'Off' time of 45 seconds were used. The recesses were filled in 5 days. Composition along the length of the microposts was analyzed using an electron microprobe and are shown in Figure 5.15. The analyses showed that the alloy is homogeneous along the length of the microposts with a mean composition of 3.31 wt % W and a standard deviation of 0.42. Thus it can be concluded that microposts with homogeneous composition of Ni-W alloy can be obtained by constant current pulsing.

The microhardness was tested and found to be 640 Knoop on top of the post and 580 Knoop on the sidewalls. This value is roughly 2 times the value of Ni reported from citrate electrolytes[25] and three times the hardness of an electrodeposited Ni from a sulfamate bath[26]

Figure 5.12: Optical picture of 200 μm tall microposts obtained from Bath #4 by constant current pulsing with a duty cycle of 0.2, pulse current of 16.5 mA/cm^2.

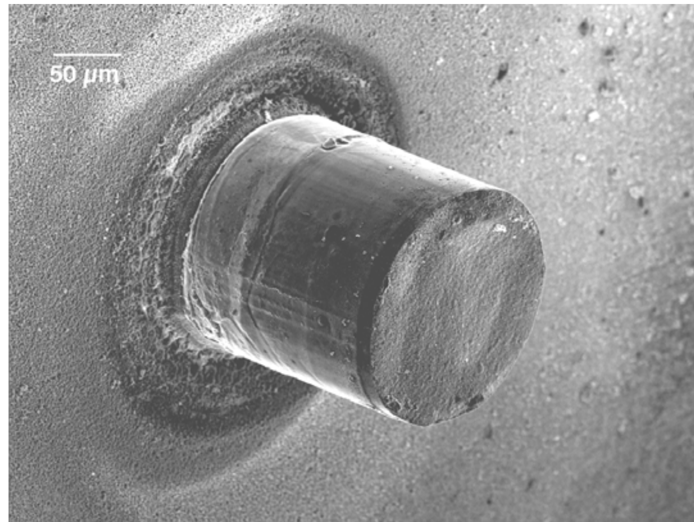

Figure 5.13: SEM image of a micropost obtained from Bath #4 by constant current pulsing with a duty cycle of 0.2, pulse current of 16.5 mA/cm^2.

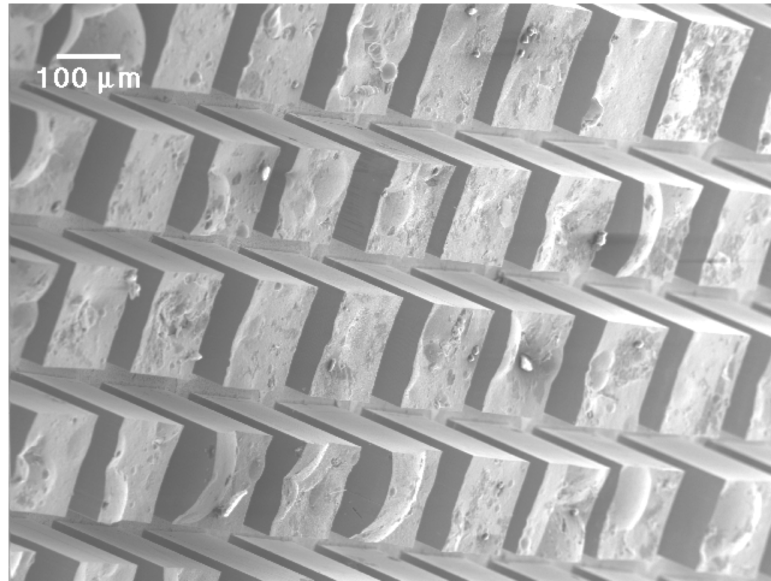

Figure 5.14: SEM micrograph of microposts grown half way, obtained from Bath #4 by constant current pulsing with a duty cycle of 0.25, pulse current of 17.5 mA/cm^2.

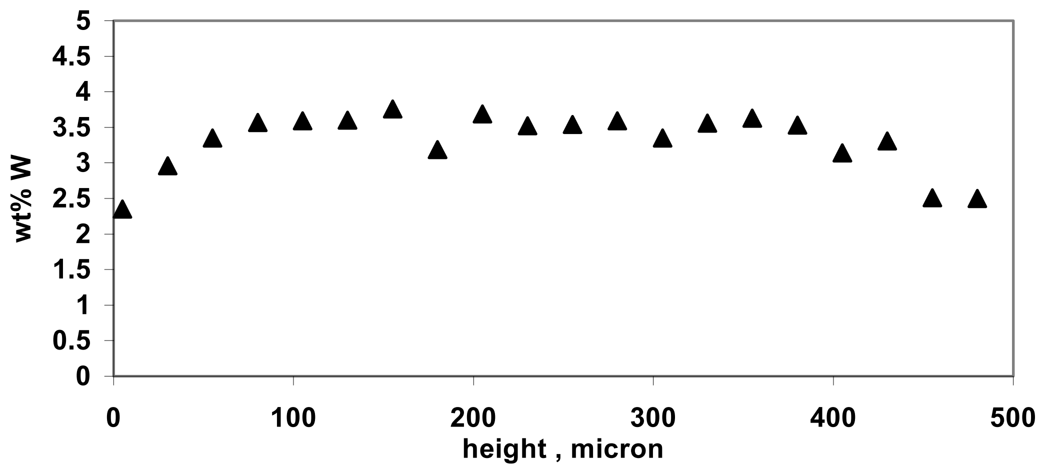

Figure 5.15 Uniform composition gradient along the length of the microposts obtained from Bath #4 by constant current pulsing with a duty cycle of 0.25, pulse current of 17.5 mA/cm^2.

5.2.3 Galvanostatic Step Ramp Pulsing

Although, constant current pulsing produces good results, it suffers from a major drawback of requiring long processing times. Optimizing the 'On' current density and

‘Off’ time could only reduce the overall processing time by a narrow margin. However, a large improvement could be made by realizing that as the recess becomes filled, the boundary layer thickness decreases and hence the limiting current of the metal reaction increases. This implies that the ‘On’ current density is less constrained and it can be increased as the deposit grows to reduce the processing time.

Hence, galvanostatic step ramp pulsing was implemented by increasing the current in steps, as shown by the schematic in Figure 5.16. An experiment was conducted with 4 steps in the pulse current. Current densities of 5 mA/cm^2, 10 mA/cm^2, 15 mA/cm^2, 20 mA/cm^2, were pulsed for 8, 8, 8, 48 hours respectively with a duty cycle of 0.25, ‘On’ time of 10 sec and ‘Off’ time of 30 sec. Microposts were grown at a rate of 166 μm/day and a 40 % saving in processing time was accomplished. Figure 5.17 shows the resulting SEM image of microposts. The deposits were analyzed for W composition along the length of the microposts. Composition variance was measured, displayed in Figure 5.18. The analyses revealed that the tungsten weight % increased at each change in current step, but decreased during the duration of each step. The decrease in W content is suspected to be due to an increase in local surface pH. Hubbard[18] showed that the W percent was directly related to pH and decreased as the bulk pH was increased by the addition of ammonia. While, this scheme disturbed the composition profile, it was able to reduce the overall processing time by 40 %.

Taking into consideration this peculiar behavior, an attempt was made to obtain a deposit with graded composition of W along the length of the microposts by increasing the number of steps in the ramp to 14. Current density was stepped by 0.75 mA/cm^2 in the current density range 5 mA/cm^2 to 15.5 mA/cm^2 every 4 hours. Microposts were grown at a rate of 117.85 μm / day. A cross section of the microposts mounted in epoxy for microprobe analysis is shown in Figure 5.19. This attempt proved successful by obtaining a graded W composition in the microposts as shown in Figure 5.20. The composition of W can be controlled where it is nearly zero at the bottom and progressively increases to 5 wt %. Thus, it can be concluded that by varying parameters like current density, ‘On’ time, ‘Off’ time, duty cycle we could not only reduce the processing time but also control the composition of the alloy.

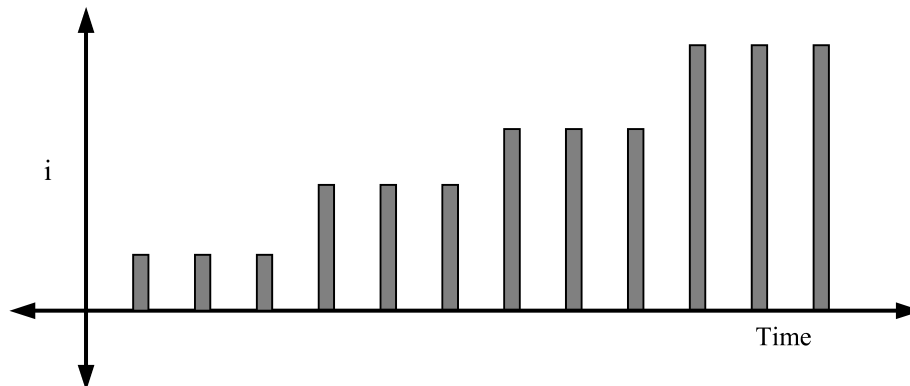

Figure 5.16: Schematic of galvanostatic step ramp pulsing.

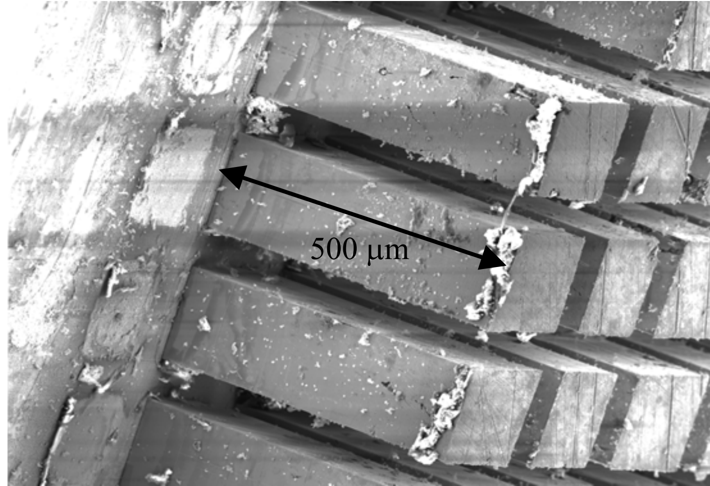

Figure 5.17: SEM image of 500 μm tall microposts' cross-section obtained from Bath #4 by galvanostatic step ramp pulsing with a duty cycle of 0.25.

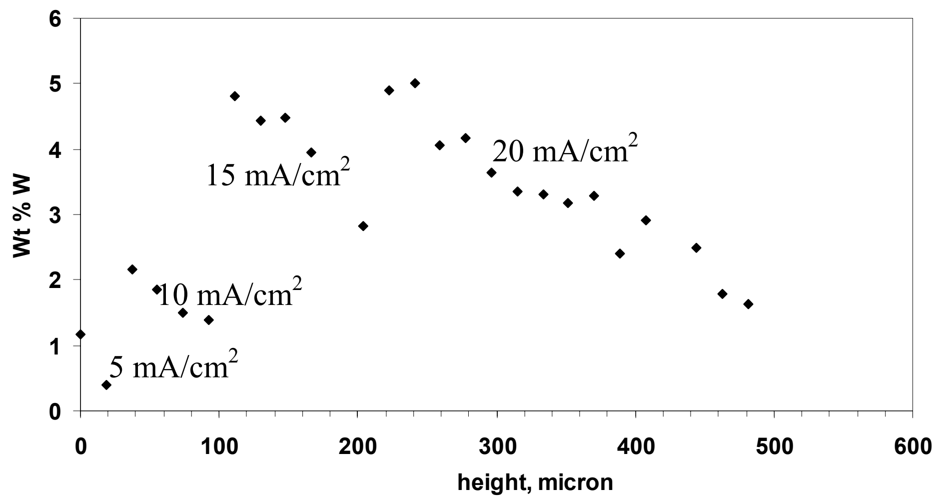

Figure 5.18: Weight percent W along the length of the microposts obtained from Bath #4 by galvanostatic step ramp pulsing with a duty cycle of 0.25.

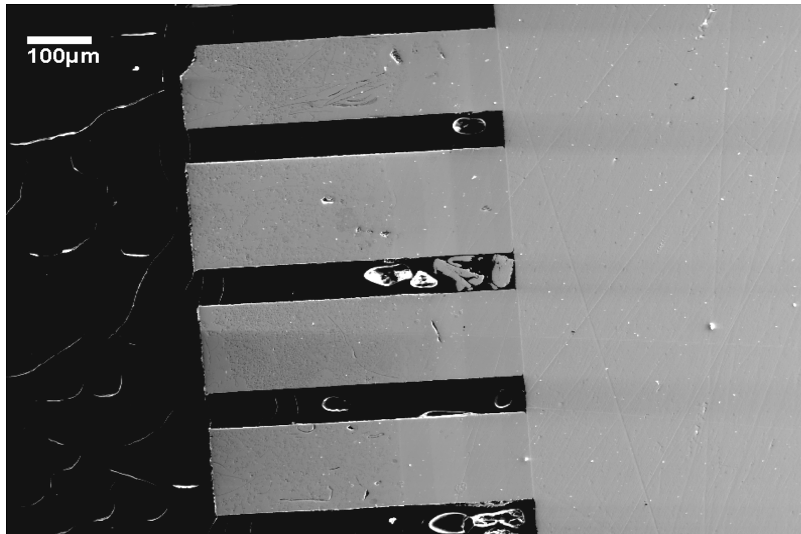

Figure 5.19: SEM micrograph of of 500 μm tall microposts' cross-section obtained from Bath #4 by galvanostatic step ramp pulsing with a duty cycle of 0.25.

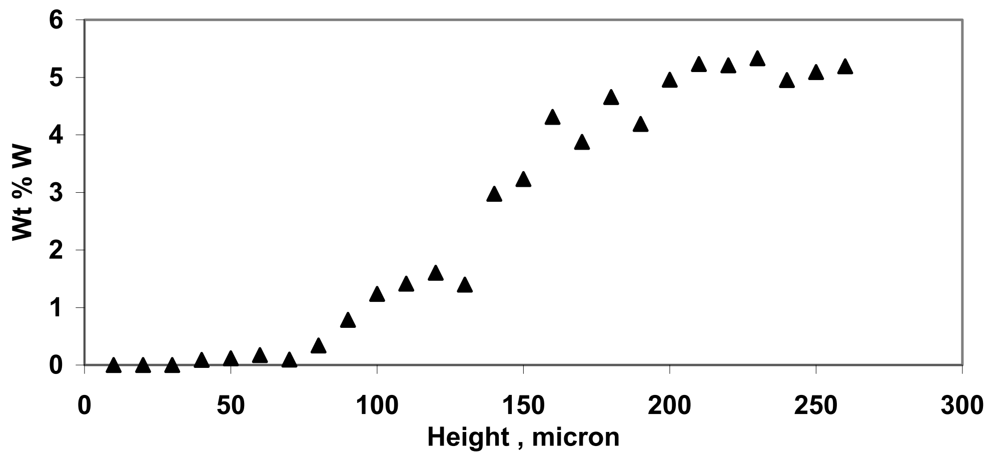

Figure 5.20: Weight percent W along the length of the microposts obtained from Bath #4 by galvanostatic step ramp pulsing with a duty cycle of 0.25.

5.2.4 Constant Current Pulsing with Reduction in 'Off' Time with Time

Another methodology to reduce the overall processing time is to reduce the 'Off' time with the growth of the deposit. A schematic of this scheme is shown in Figure 5.21. As, the deposit grows the boundary layer thickness decreases. Hence, the time required to attain equilibrium during the 'Off' time in the recess is less constrained. Thus a saving in the processing time could be made by not only varying the 'On' current density but also reducing the 'Off' time as the deposition progresses.

This scheme was implemented with the same conditions used for constant current pulsing with the square mesh pattern, as described in 5.2.3. Retaining the 'On' time of 15 sec, a change in the 'Off' time was made to increase the duty cycle by 0.03 every 19.5 hours. A reduction of 20 % in the processing time was achieved. Deposits were grown successfully using the scheme but a composition analysis along the length of the deposit revealed that the composition is slightly disturbed as shown graphically in Figure 5.22. So, this scheme was not adequately optimized to maintain a constant composition. The duty cycle should be increased at a slower rate.

Figure 5.21: Schematic of the Pulsing Scheme showing 'Off' Time Reduction with Time

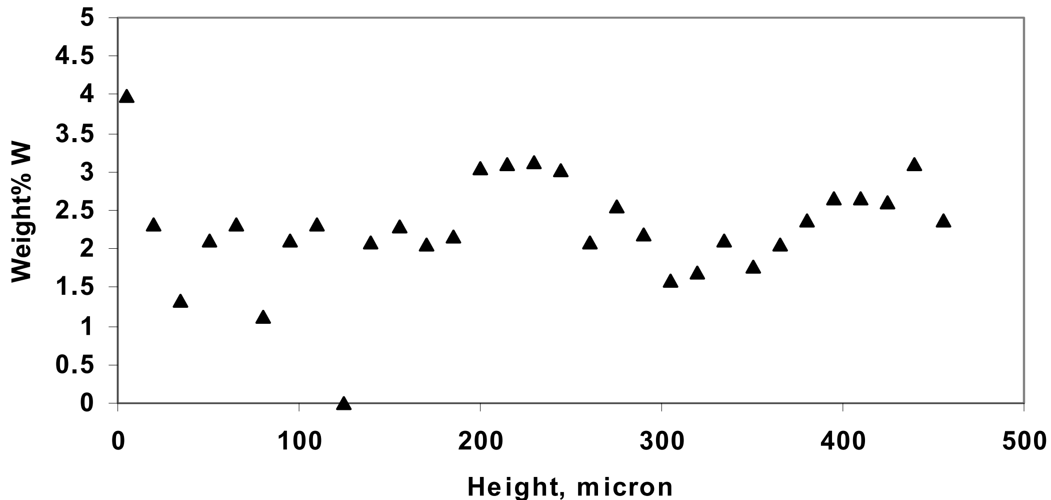

Figure 5.22: Microprobe analysis showing composition gradients in the microposts obtained by 'off' time reduction scheme

5.3 Ramping Scheme to Electrodeposit Ni into Deep Recesses

The concept of ramping the current even without the pulse to minimize the plating time can also be of interest to other elemental and alloy systems in deep recess plating. A sulfamate bath was chosen to investigate the applicability of the ramping scheme to plate pure Ni into 500 μm recesses. The composition of the sulfamate bath used is given in Table 5.1. The bath was operated at 60 °C and a pH of 4.0. The pH of the bath was made

up using sulfuric acid. Ni is conventionally plated into deep recesses at 20 mA/cm^2 and the deposits grow at a rate of 25 μm per hour. Current was ramped from 20 mA/cm^2 to 116 mA/cm^2 at a rate of 12 mA/cm^2 per hour. The schematic of the ramping scheme is shown in Figure 5.23. Figure 5.24 shows the SEM picture of the Ni microposts obtained by this scheme. It took 8 hours to fill the 500 μm recesses as opposed to 20 hours by dc plating, saving more than 50 % of the plating time. Thus we can conclude that the ramping scheme is also applicable to the electrodeposition of Ni into deep recesses.

Table 5.1: Composition of Sulfamate Bath used for electroplating Ni into 500 μm Recesses

Component	Concentration
Nickel sulfamate	450 g/l
Boric acid	37.5 g/l
Saccharin	4 g/l
Sodium dodecyl sulfate	1 g/l

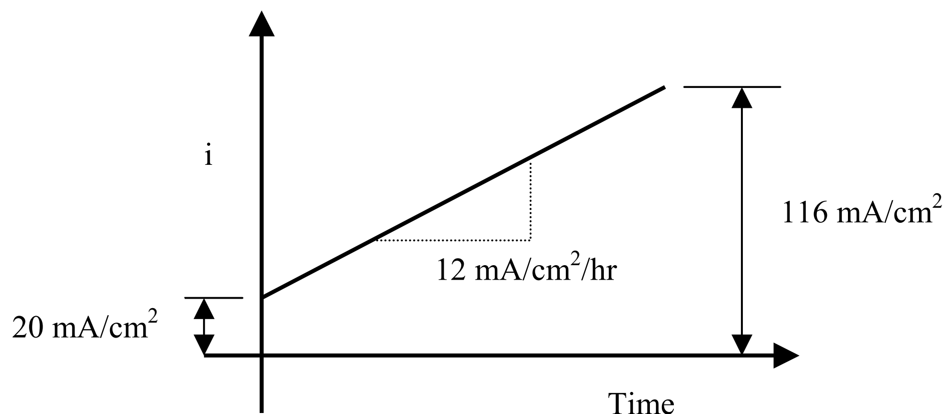

Figure 5.23: Schematic of the ramping scheme used to plate Ni into 500 μm recesses.

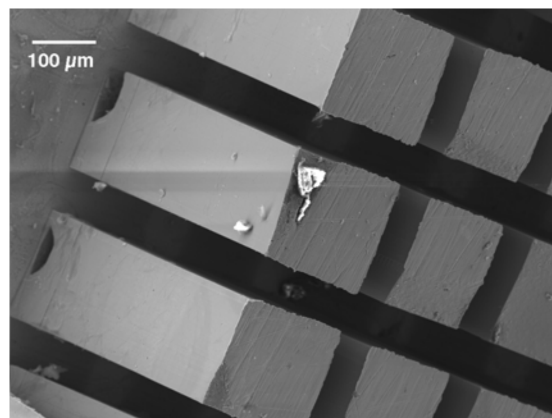

Figure 5.24: SEM micrograph of Ni microposts obtained from sulfamate bath by using the ramping scheme in Figure 5.22

5.4 Pulsing Scheme to Electrodeposit Ni-Fe Alloy into Deep Recesses

In an effort to demonstrate that the devised pulsing scheme is also applicable to deposit other alloys into deep recesses, a bath containing nickel sulfamate and ferrous sulfate was chosen to deposit iron-rich Ni-Fe alloy. This bath was adapted from Datta's thesis.[27] Chloride salts were replaced by sulfate salts and more iron salt was added to achieve composition that of invar. The composition of the bath used is given in Table 5.2. The bath was operated at 40 °C and a pH of 2 which is adjusted

Table 5.2: Composition of Ni-Fe Electroplating Bath

Nickel Sulfamate	0.72 M
Ferrous Sulfate	0.147 or 0.155 M
Boric Acid	0.5 M
Sodium Lauryl Sulfate	0.001 M
Ascorbic Acid	0.011 M
Saccharin	0.008 M

with sulfamic acid. Plating was carried out at 8.5 mA/cm^2 with a duty cycle of 0.25, 'On' time of 10 seconds and 'Off' time of 30 seconds. The plating resulted in successful growth of shiny and stress-free Ni-Fe microposts. An SEM image of the Ni-Fe microposts obtained is shown in Figure 5.25. Without a pulsing method, at this current density no deposit could be grown in the 500 μm recesses. The composition of iron in the deposit was sensitive on the composition of iron in the solution.A deposit of 58 wt % Fe was obtained with the 0.147 M $FeSO_4$ and a value of 64 wt % Fe was found at 0.155 M $FeSO_4$. Figure 5.26 shows 500 μm Ni-Fe posts with 64% Fe. The 64 wt % Fe is significant since it is the composition where a low coefficient of thermal expansion occurs. Commonly referred to as Invar, at this composition the magnetic effects balance the thermal effects restricting its expansion. Above the Curie temperature (200 ^{0}C), where ferromagnetism disappears, the alloy expands normally.

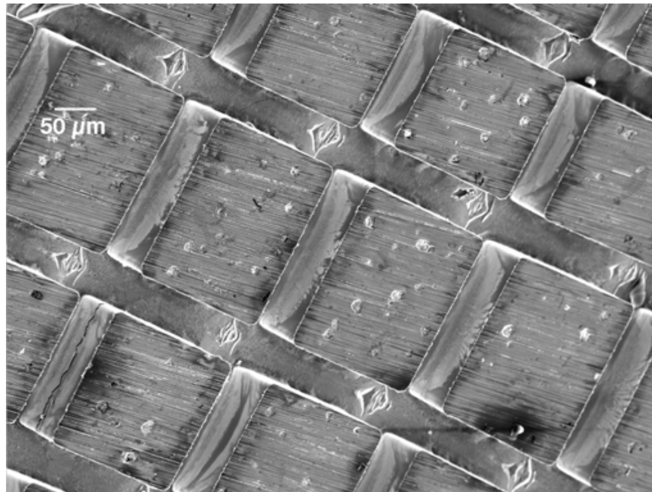

Figure 5.25: SEM image of 100 μm tall Ni-Fe Microposts with 58 % Fe obtained by Pulse Plating

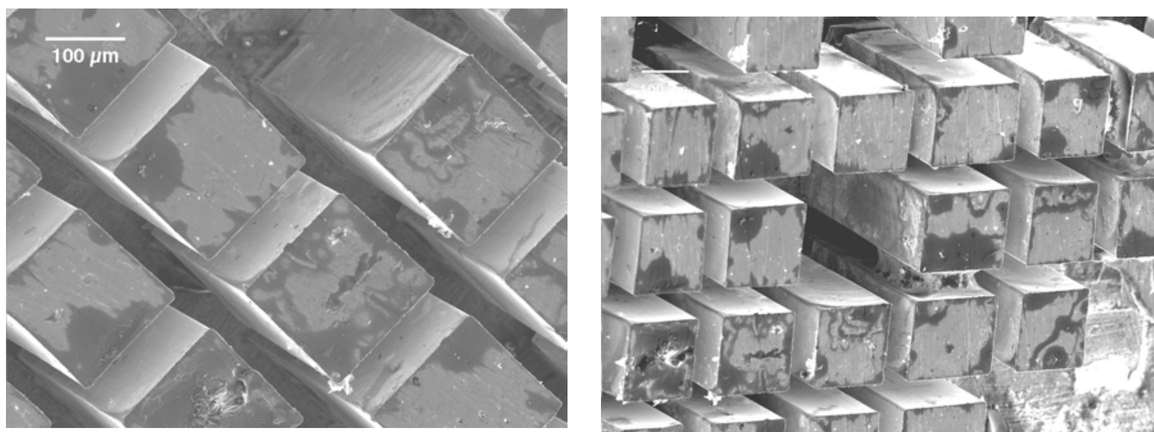

Figure 5.26: SEM images of 500 μm tall Ni-Fe Microposts with 64 % Fe obtained by Pulse Plating

5.5 Experiments on Rotating Cylinder Electrodes

The electrolyte used for microstructure development was investigated for composition, current efficiency and partial currents of different reactions occurring by carrying out plating onto cylinder electrodes at different rotation rates. The results obtained are shown in Figures 5.27, 5.28, 5.29, and 5.30. It was observed that there is a slight dependence of the alloy the composition dependency with current density, up to a limiting value. The current efficiency as a function of applied current density was found to be independent of rotation rate.

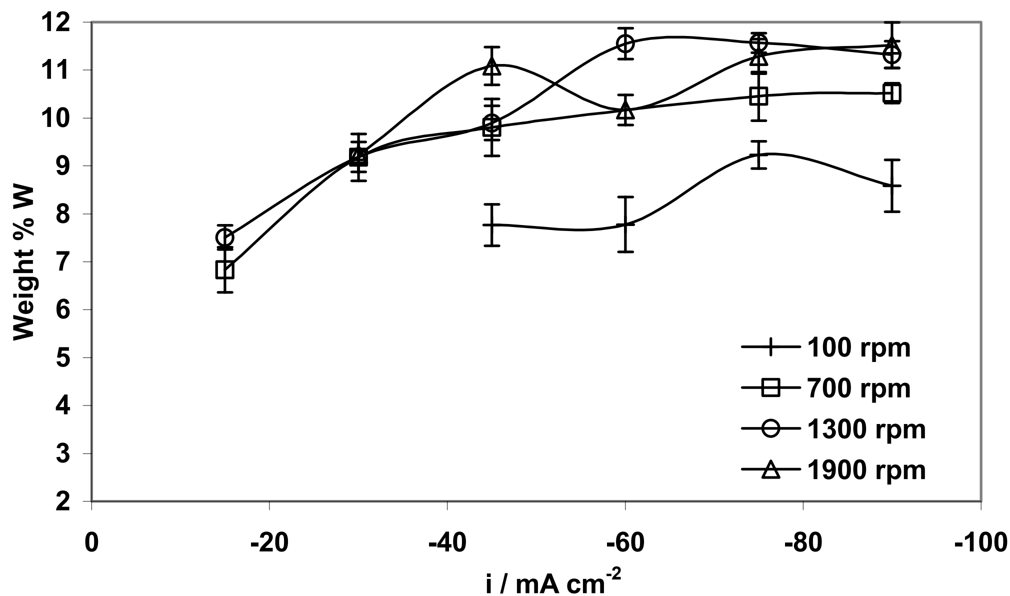

Figure 5.27: Weight percent tungsten vs. applied current density at rotation rates of 100, 700, 1300 and 1900 rpm for Bath #4, (Intermediate), pH of 10, at 70 °C.

The partial current densities are shown in Figures 5.28 and 5.29. A positive shift in the reduction potentials was observed with an increase in rotation rate for the Ni, W (Figure 5.28) and side reactions (Figure 5.29). The shift is not common in alloy plating and has been observed only for the NiW system.[18]

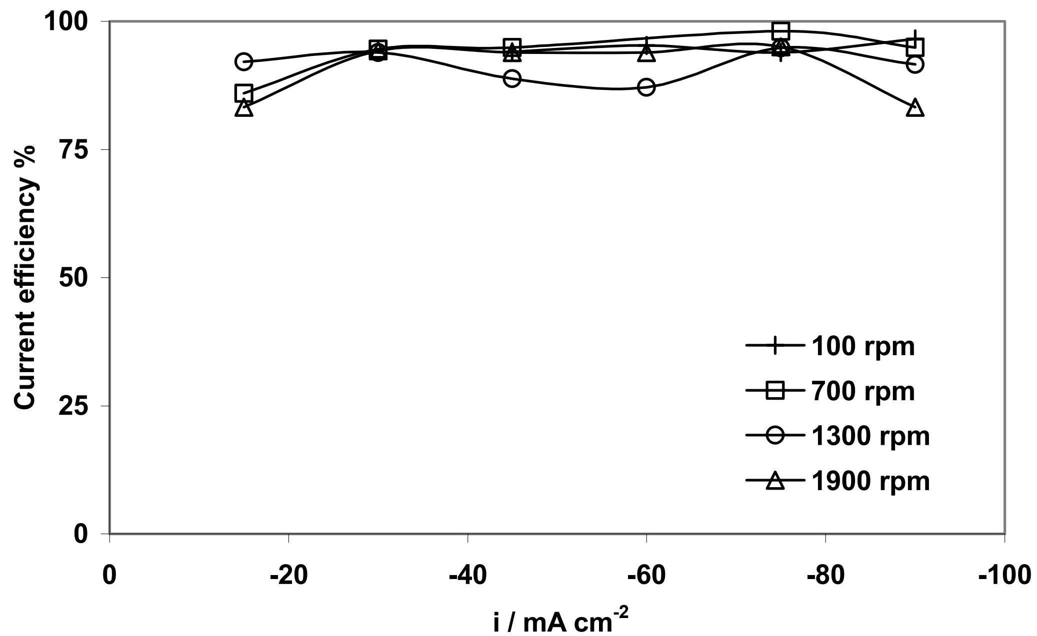

Figure 5.28: Current efficiency vs. applied current density at rotation rates of 100, 700, 1300 and 1900 rpm for Bath #4, (Intermediate), pH of 10, at 70 °C.

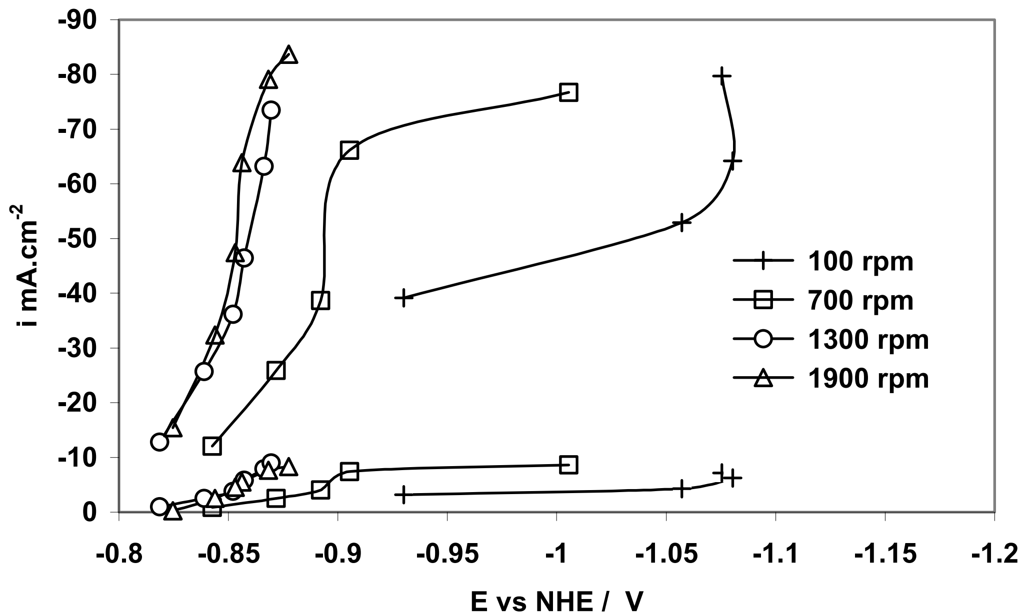

Figure 5.29: Partial current densities of Ni and W vs. potential at rotation rates of 100,700, 1300 and 1900 rpm for Bath #3, (Intermediate), pH of 10, at 70 °C.

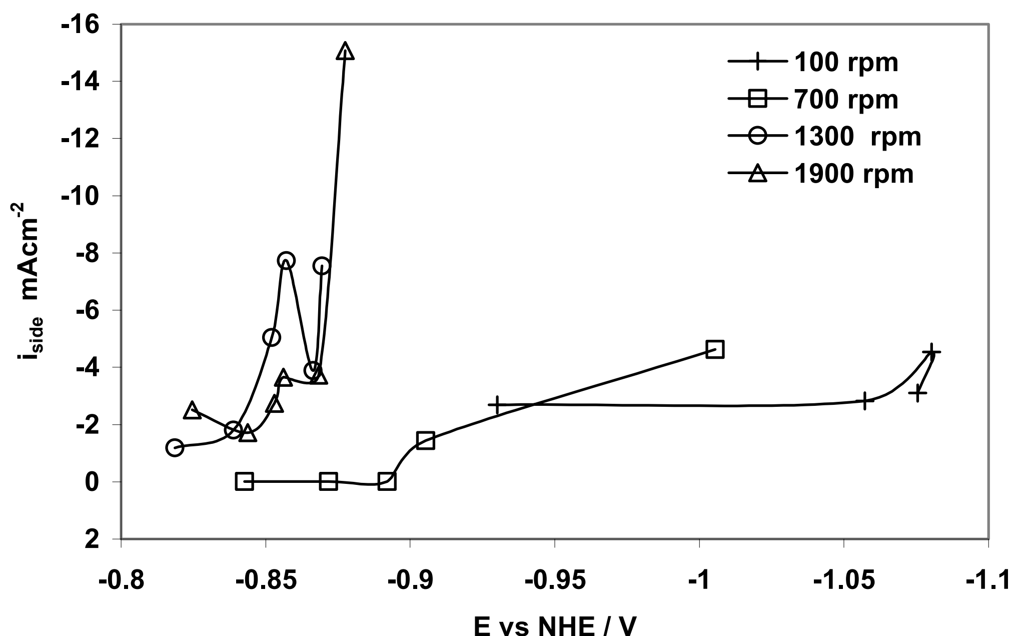

Figure 5.30: Partial Current Densities of Side Reaction vs. Potential at rotation rates of 100, 700, 1300 and 1900 rpm for Bath #3, (Intermediate), pH of 10, at 70 °C.

5.6 Effect of Ni Concentration on NiW Electrodeposition

Results from three electrolytes, Bath #1, Bath #3 and Bath#4 having concentrations of 0.4 M, 0.2 M, 0.1 M nickel sulfate were compared to study the effect of Ni concentration on composition of alloy, and current efficiency. Figure 5.31 shows that there is no particular trend in the composition of alloy with respect to nickel concentration of the electrolyte. Current efficiency as a function of current density for different baths is shown in Figure 5.32. At lower current densities, higher current efficiencies were observed for all the electrolytes, but with the increase in current density, higher current efficiencies were obtained from higher nickel concentration electrolytes.

5.7 Effect of Tungstate Concentration on NiW Electrodeposition

An electrolyte with the same composition as of Bath #1, but with double the concentration of sodium tungstate was examined to study the change in the composition of the alloy. An increase in the concentration of sodium tungstate did not change the composition of the alloy as is illustrated in Figure 5.33. Also, the current efficiency of the deposition process did not vary significantly with the increase in tungstate concentration as shown in Figure 5.34. Essentially, there was no change in the partial currents of any species, particularly W, despite the fact that tungstate concentration was doubled. Thus it can be concluded that the composition of the deposit and current efficiency of the process are independent of the tungstate concentration of the electrolyte when the concentration of other species are kept constant.

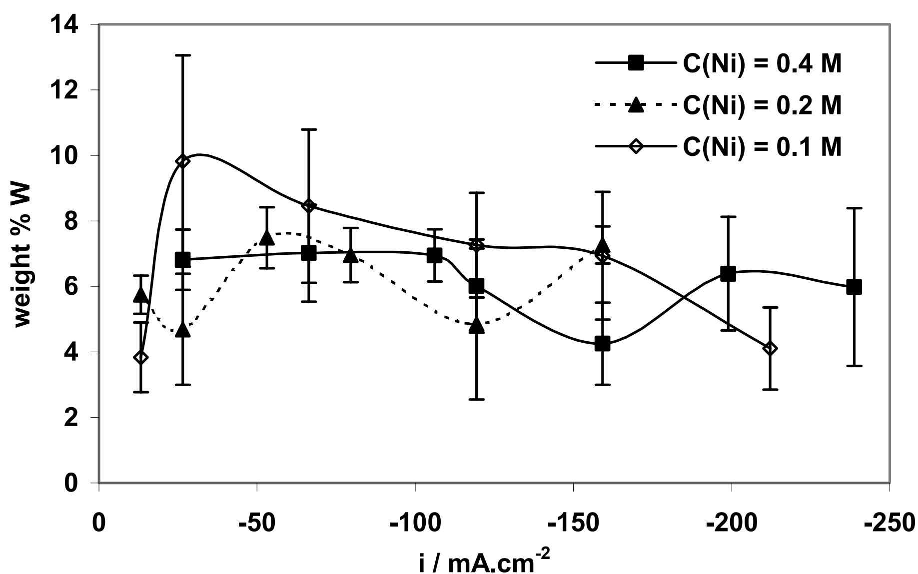

Figure 5.31: Weight Percent W vs. Current Density for Bath #1, Bath #3 and Bath #4 at 300 rpm, pH of 10, and at 70 °C

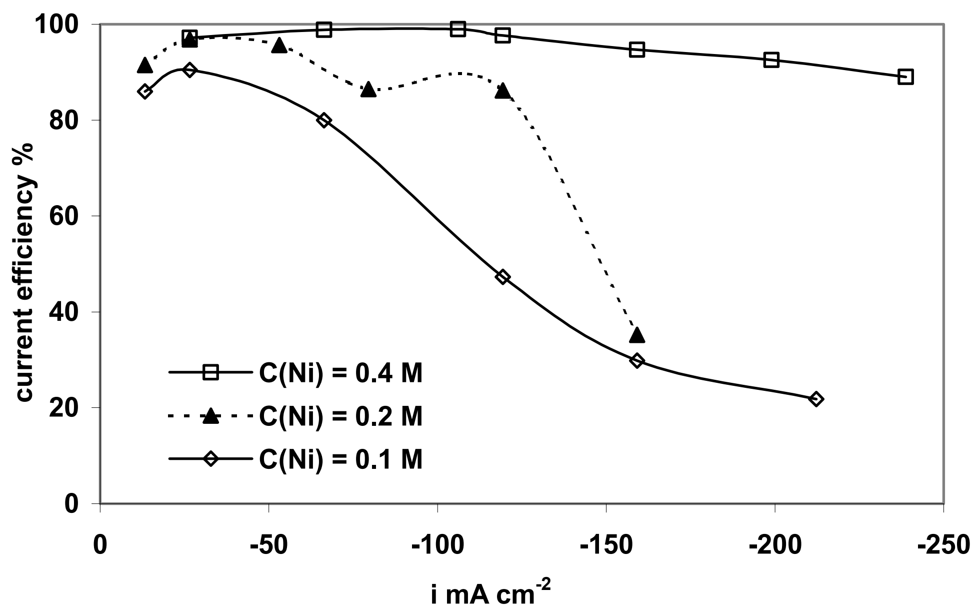

Figure 5.32: Current Efficiency vs. Current Density for Bath #1, Bath #3 and Bath #4 at 300 rpm, pH of 10, and at 70 °C, different Ni concentrations of the electrolyte

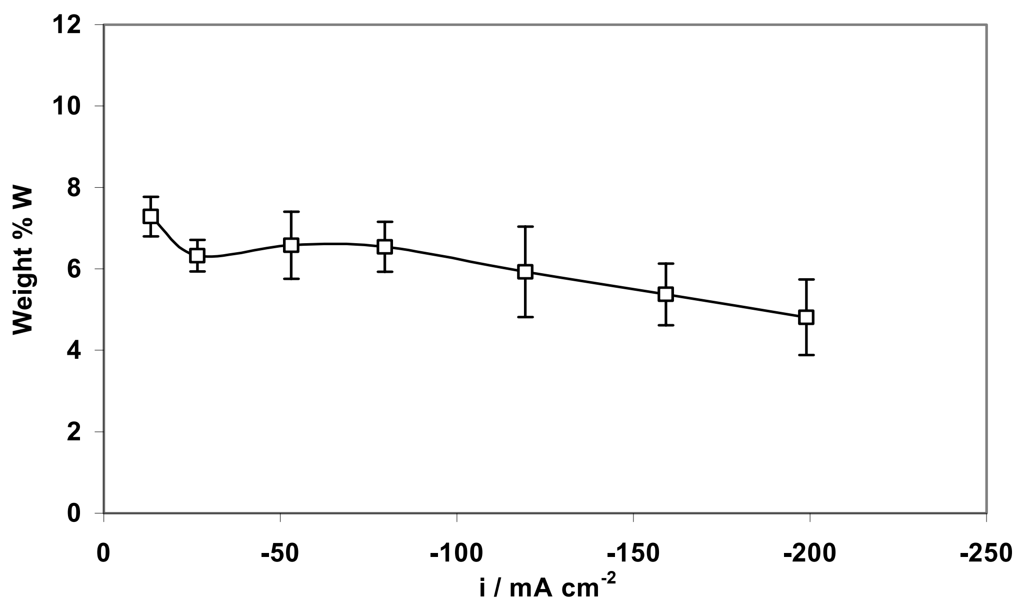

Figure 5.33: Weight Percent W as a function of applied current density for Bath #2 (Double Tungsten) at 300 rpm, pH of 10, at 70 °C.

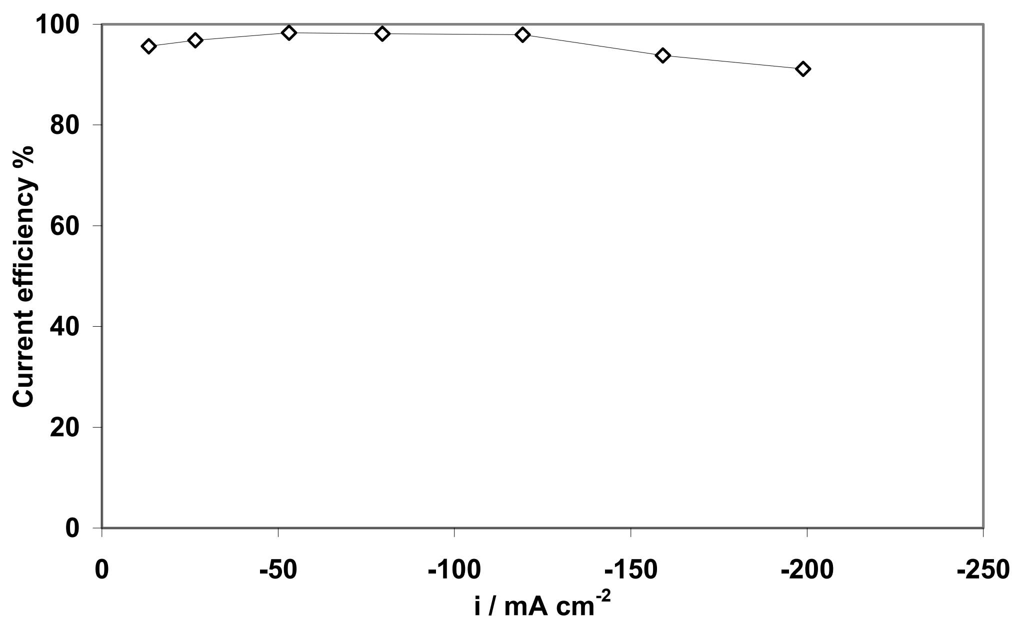

Figure 5.34: Current efficiency as a function of applied current density for Bath #2 (Double Tungsten) at 300 rpm, pH of 10, at 70 °C.

CHAPTER 6.   CONCLUSION

In this thesis work, Ni-W alloys were electrodeposited into 500 µm deep recesses with a control in composition using pulse plating with a long off time. A citrate-based electrolyte was chosen for this purpose. It was identified that pulse plating with a long relaxation time is the key feature to counteract the problems associated with local pH rises and diffusion of side products inherent with NiW alloy electrodeposition into deep recesses. Success was found with galvanostatic pulsing over potentiostatic pulsing.

NiW microstructures, 500 µm tall with 3.37 weight % W and a microhardness of 600 Knoop were obtained in 5 days by galvanostatic pulsing. The hardness is more than three times greater than nickel deposits from sulfamate electrolyte, used presently in microdevices. Galvanostatic step ramp pulsing and Off-time reduction schemes were devised and implemented to shorten the processing time. Electrodeposition was successful using these schemes but composition was disturbed.

Galvanostatic step ramp pulsing could also be used to control the composition of the alloy in the recess. Microposts with a graded composition along the length of micropost were obtained by this scheme. Thus was demonstrated that the composition of the alloy in the recess could also be controlled by varying the plating parameters from a single electrolyte.

Ni-Fe microposts with composition close to that of Invar were also obtained by using pulse plating routines. Thus, this study demonstrates that the pulsing schemes devised could be used as a general method to deposit many other alloy systems into deep recesses.

In addition, it was shown that a galvanostatic ramping scheme could be used to plate pure Ni into 500 µm deep recesses with a 50 % saving in the deposition time. The ramp takes advantage of a growing boundary layer that limits the reaction rate. RCE experiments on electrolyte used for microstructure development indicate that there is no effect of rotation rate on current efficiency, which shows that the deposition is not mass transport controlled. However, a positive shift in the reduction potentials was observed with increase in rotation rate. The shift in potential therefore explains the difficulty in plating into recesses under potentiostatic control, in addition to an ohmic potential control. Composition of the alloy is found to be independent of Ni concentration in the electrolyte chosen.

REFERENCES

1. H. Lowe, W. Ehrfeld and J. Diebel, Proceeding of SPIE, **3223**, 168 (1997).

2. R. M. Krishnan, C. Joseph Kennedy, Sobha Jay A. Krishnan, S. Sriveeraraghavan, and S. R. Natarajan, *Metal Finishing,* **93** (7), 33 (1995).

3. L. T. Romankin, *Electrochemica Acta*, **42**, 2985 (1997).

4. W. Erhfeld, V. Hessel, H. Lowe, Ch. Schultz and L. Weber, *Microsystem Technologies*, **5**, 105 (1999).

5. J. Gottert, Presentation at the 1st Annual Louisiana Microsystems Conference at the Institute for Micromanufacturing, Louisiana Tech University, Ruston, (April, 2000).

6. A. Brenner, Electrodeposition of Alloys, Academic Press, New York, **vol.2**, 345, (1963).

7. A. Brenner, Electrodeposition of Alloys, Academic Press, New York, **vol.1**, 75, (1963).

8. M. Bratoeva and N. Atanassov, *Metal Finishing*, **96**, 92 (1998).

9. L. E. Vaaler and M. L. Holt, *Trans. Electrochem. Soc.,* **90**, 43 (1946).

10. O. Younes and E. Gileadi, *Electrochemical and Solid State Letters*, **3** (12), 543 (2000).

11. V. B. Singh, L. C. Singh and P. K. Tikoo, *J. Electrochem. Soc.*, **127** (3), 590 (1980).

12. M. Obradovic, J. Stevanovic, A. R. Despic, and R. Stevanovic, *J. Seerb. Chec. Soc.*, **64** (4), 245 (1999).

13. T. F. Fransevich-Zabludovskaya, A. I. Zayats, Zh. Priklad.Khim., **30**, 723 (1957).

14. N. Atanassov, K. Gencheva, and M. Bratoeva, *Plating and surface finishing*, **84** (2), 67 (1997).

15. D. R. Gabe, *J. Appl. Electrochem.,* **27**, 908 (1997).

16. E. J. Podlaha and D. Landolt, *J. Electrochem Soc*., **143** (3), 885 (1996).

17. B. N. Maruthi, L. Ramesh, S. M. Mayanna and D. Landolt, *Plating and Surface Finishing*, **86** (3), 85 (1999).

18. P. B. Hubbard, MS Thesis, Department of Chemical Engineering, Louisiana State University, (2000).

19. M. Kupper and J. W. Schultze, *Electrochemica Acta*, **42**, 3023 (1994).

20. A. M. Bond, D.Luscombe, K. B. Oldham and C. G. Zoski, *J. Electroanal. Chem*., **249**, 1 (1998).

21. J. C. Puippe, *Plating and Surface Finishing,* **73** (8), 36(1986).

22. N. IBL, *Surface Technology*, **10**, 81 (1980).

23. D. Landolt, *ElectrochemicaActa*, **39**, 1075 (1994).

24. C. M. A. Brett and A. M. O. Brett, Electrochemistry: Principles, Methods, and Applications, Oxford University Press, Inc., New York, 253 (1994).

25. Christian Bonhote, Ph.D. Thesis, "Electrodeposition de Multicouches Ni-Cu Nanomodulees a Partir d'un Bain de Citrate et Etude de Leurs Propriétés Mécanique, Ecole Polytechnique Federale de Lausanne, Switzerland, 125 (1995).

26. D. Simunovich, M. Schlesinger and D.D. Snyder, "Electrochemically Layered Copper-Nickel Nanocomposites with Enhanced Hardness," *J. Electrochem Soc*., 141-1 (1994).

27. P. Datta, MS Thesis, Department of Mechnical Engineering, Louisiana State University, (2001).

VITA

Lakshmikanth Namburi was born on September 30, 1977, to Krishna Kumar Namburi and Savitri Namburi in Sakhinetipalli, Andhra Pradesh, India. He chose chemical engineering as his major field of study and went to Chaitanya Bharathi Institute of Technology, Osmania University for his undergraduate study. He graduated in May 1999 as the topper in his class with a gold medal, earning a bachelor of technology degree in chemical engineering. After his undergraduation, he came to the United States of America for pursuing his graduate studies in chemical engineering at Louisiana State University in August 1999. In December 2001, he will receive the degree of Master of Science in Chemical Engineering. He is currently employed as a process engineer with Teravicta Technologies Inc. located in Austin, Texas.